

Quantification of ground movement

State-of-the-art

Deliverable No.:	D1.1	Responsible for deliverable:	NGI
Quality control by:	NGI, Lars Grande	Contributing partner(s):	BGS, GEOMAR, NGI, QUAD Geometrics,
Deliverable prepared by:	Bahman Bohloli, Per Magnus Sparrevik, Malte Vöge, Regula Frauenfelder, Joonsang Park, Christian Berndt, Luke Bateson, Jens Karstens, Ekbal Hussain, Alessandro Novellino	Dissemination level:	Open Access
Project No.:	299664	Date:	2020-01-20 Rev. No.: 0

This project, SENSE, is funded through the ACT programme (Accelerating CCS Technologies, Horizon2020 Project No 294766). Financial contributions made from The Research Council of Norway, (RCN), Norway, Gassnova SF (GN), Norway, Bundesministerium für Wirtschaft und Energie (BMWi), Germany, French Environment & Energy Management Agency (ADEME), France, US-Department of Energy (US-DOE), USA, Department for Business, Energy & Industrial Strategy (BEIS) together with extra funding from NERC and EPSRC research councils, United Kingdom, Agencia Estatal de Investigación (AEI), Spain, Equinor and Quad Geometrics are gratefully acknowledged.

Project information

Project title: Assuring integrity of CO₂ storage sites through ground surface monitoring (SENSE)
Project period: 1 September 2019-30 August 2022
Project Coordinator: Norwegian Geotechnical Institute
Web-site: <https://sense-act.eu/>

Project partners



Funding Agencies



This document reflects only the authors' view and that the funding agencies are not responsible for any use that may be made of the information it contains.

The present document has not yet received final approval from ACT and may be subject to changes.

Contents

1. Introduction.....	5
2. Monitoring methods for CO2 storage sites.....	6
2.1 In Salah CO2 storage site, Algeria.....	8
2.2 Illinois Basin-Decatur Project, USA.....	8
2.3 Quest Project, Canada.....	9
2.4 Sleipner CO2 storage, Norway.....	10
2.5 Snøhvit CO2 storage, Norway.....	11
3. Satellite-based ground monitoring.....	13
3.1 SAR Interferometry in CO2 storage applications.....	13
3.2 The Persistent Scatterer technique (PS).....	18
3.3 The Small BAseline Subset technique (SBAS).....	18
3.4 Data.....	19
4. Seafloor deformation monitoring.....	21
4.2 Repeated bathymetric and seismic surveys.....	23
4.2.1 4.1.1 Bathymetric surveys.....	23
4.2.2 Seismic surveys.....	25
4.3 Direct seabed deformation measurements.....	27
4.3.1 Long-distance acoustic direct-path long ranging network.....	27
4.3.2 Short distance acoustic direct-path distance ranging networks.....	29
4.3.3 NGI Fault extensometers.....	30
4.3.4 Seismic recorders.....	31
4.3.5 Ocean bottom pressure recorders.....	32
4.3.6 Seabed tiltmeters.....	35
4.3.7 Benchmark foundations.....	37
4.3.8 Baseline profiling using closed circuit liquid pressure systems.....	39
4.3.9 Baseline profiling using fibre optic strain cables.....	40
4.4 Systems proposed for testing and evaluation at seafloor in SENSE.....	44
4.4.1 Suction bucket foundations.....	Error! Bookmark not defined.
4.4.2 Combined tilt and pressure recording unit (Geomar).....	45
4.5 Fibre optic seabed cable for distributed sensing (NGI).....	46
References.....	48
Appendix A – InSAR Terminology and Working Concept.....	57
A1. InSAR Terminology.....	57
A2. Spatial Resolution.....	59

A3. Further principles of SAR Interferometry.....	60
A4. Image Coherence.....	62
A5. InSAR data processing	64
A6. InSAR stack processing	65

1. Introduction

Geological sequestration of anthropogenic CO₂ is one of the key solutions for a low carbon future. The IEA ETP report indicates that more than 90 Giga tonnes of carbon dioxide will need to be stored underground by 2050 in order to meet the 2 °C climate target. To meet this target, 100s of millions of tonnes of CO₂ should be captured and stored annually at many sites over several decades. Scaling up the rates and number of injection sites in order to meet climate targets requires that monitoring, verification, and performance management moves from a small number of intensively monitored pilot and demonstration projects to full-scale Giga tonne deployment (Mission Innovation CCUS, 2017). This highlights the need for monitoring of large areas (tens of square kilometres), at reasonable cost and appropriate temporal and spatial resolutions.

Monitoring of geological CO₂ storage sites is crucial for gaining acceptance of CO₂ storage as a reliable method for reducing CO₂ emissions as well as for verification of site behaviour and to enable storage site closure in the long term. Monitoring plans for such large-scale storage sites need to include both the injection and post-injection phases to assure CO₂ is stored over geological timescales and effectively monitored in the subsurface. A bottleneck for deployment of CCS is the economics of operation including the high cost for storage site monitoring. The ambitious goals of SENSE project is to demonstrate how ground surface movement can be used as an integral part of the monitoring program to effectively verify safe storage of CO₂ underground.

The proposed SENSE research activities are focused towards injection demonstration sites both onshore and offshore. Therefore, review of the existing technology for data acquisition and reporting the state-of-the-art is the first step on this path. This report will summarize the ready-to-use techniques for acquiring data on ground motion, including those which have been selected for application through SENSE. After a short review of monitoring plans for selected CO₂ storage pilots/projects in Section 2, Section 3 reviews the status of monitoring terrain motion on land and Section 4 presents method and technologies available for monitoring seafloor motion.

2. Monitoring methods for CO2 storage sites

There are plenty of potential methods, developed mainly by the oil and gas industry, that can be adapted for monitoring CO2 storage sites. Hence, the monitoring programmes are usually site specific adopted to the risks, benefits, costs and purpose (Chadwick et al. 2008, IEAGHG 2011, Wright et al. 2017, Eide 2012). IEAGHG (2011) presented a suite of monitoring methods for onshore and offshore sites (Fig. 2.1). The focus of SENSE is on ground level monitoring using remote sensing and other techniques; including Interferometric Synthetic Aperture Radar -InSAR (marked as a "primary use" in Fig. 2.1) and seafloor movement (which has not explicitly been mentioned in Fig. 2.1).

<div style="display: flex; justify-content: space-between;"> <div style="width: 45%;"> <p> Onshore only</p> <p> Onshore & Offshore</p> <p> Primary use</p> <p> Secondary use</p> <p> New addition or change to table</p> </div> <div style="width: 45%; text-align: center;"> <p> Offshore only</p> </div> </div>			Deep	Shallow	Plume location/migration	Fine-scale processes	Leakage	Quantification	New addition
Seismic		3D/4D surface seismic							
		Time lapse 2D surface seismic							
		Multicomponent seismic							
	Acoustic imaging	Boomer/Sparker							
		High resolution acoustic imaging							
	Well-based	Microseismic monitoring							
		4D Cross-hole seismic							
4D VSP									
Sonar Bathymetry	Sidescan sonar								
	Multi beam echo sounding								
Magnetics*	Airborne magnetic								
	Ground magnetic								
	Magnetic gradiometry								
Gravimetry	Time lapse surface gravimetry								
	Time lapse well gravimetry								
Electrical/Electro-magnetic	Surface EM								
	CSMT								
	Magnetotellurics								
	Sea bottom EM (CSEM)								
	Cross-hole EM/imaging								
	Permanent borehole EM								
	Cross-hole ERT								
ESP									
Remote sensing	Airborne hyperspectral imaging								
	Satellite interferometry								
	Airborne EM								
Others	Geophysical logs**								
	Pressure/temperature								
	Differential GPS								
	Tiltmeters								
	Magnetic Resonance Sounding								
	Borehole NMR								
	GPR - surface								
	GPR - borehole (tomography)								

*Used to map faults/potential leakage points
 ** Geophysical logs included gamma, resistivity, neutron, gamma-gamma, induction and magnetic susceptibility
 CSMT = Controlled Source Magnetotellurics
 CSEM = Controlled Source ElectroMagnetics

Figure 2.1 Potential methods and tools for monitoring CO2 storage sites (IEAGHG 2011).

Remote sensing technologies can offer a solution for determining the location of CO₂ in the subsurface and identifying indicators that the storage complex is not behaving as expected. Remote sensing utilizes monitoring tools that can gather data across the area of interest without having to go to the site and could provide an option for non-invasive and large scale spatial monitoring (Litynski et al. 2013). Remote sensing technologies for monitoring CO₂ storage sites have been considered promising solutions and used at CO₂ storage demonstration/pilot sites around the world. The US National Energy Technology Laboratory (NETL), for instance, has invested on such technologies over the past decades. Figure 2.2 presents remote sensing technologies for monitoring, verification, accounting and assessment (MVA) of CO₂ storage sites, funded by NETL. These technologies have already been deployed at several CO₂ storage pilots/large scale sites around the world and showed great value and benefit (see sections 2.1 to 2.5).

Technology	Performer	Definition	MVA Applications	Limitations
Surface Displacement - InSAR (Interferometric synthetic aperture radar)	<ul style="list-style-type: none"> Lawrence Berkeley National Laboratory Lawrence Livermore National Laboratory University of Miami TRE Canada and BP 	Satellite-based technology used to measure surface deformation at CO ₂ injection sites.	<ul style="list-style-type: none"> CO₂ plume and pressure front tracking Detect geomechanical effects on storage formation and caprock. 	Data processing can be time consuming. Sensitive to land use changes and availability of benchmarks. Works best on level, low vegetation ground surfaces.
Surface Displacement Tiltmeter/GPS	<ul style="list-style-type: none"> Lawrence Livermore National Laboratory University of Miami Advanced Resources International 	Surface-based technology used to measure surface deformation or subsidence at CO ₂ injection sites.	<ul style="list-style-type: none"> CO₂ plume tracking Detect geomechanical effects on storage formation and caprock 	Labor-intensive process can lead to increased costs. Requires onsite surface and subsurface access. Reliability of tiltmeters can be effected by drift.
ROV (Remotely Operated Vehicles)	<ul style="list-style-type: none"> SCRIPPS 	Customizable remote platform used to conduct multiple surveys of inaccessible locations.	<ul style="list-style-type: none"> Gravity fluctuation measurements for CO₂ plume tracking Leak detection 	ROV requires a large support platform (and labor force) to conduct operations. Limited capabilities due to potential lack of attenuation.
Multi-Spectral/ Hyper-spectral Scanners (LANDSAT, SPOT, Quickbird, LIDAR)	<ul style="list-style-type: none"> Lawrence Livermore National Laboratory West Coast Regional Carbon Sequestration Partnership Midwest Geological Sequestration Consortium Nature Conservancy Montana State University University of Michigan 	Multi-platform scanner used to measure changes in floral cover, surface features, and land forms.	<ul style="list-style-type: none"> Pipeline and underground leak detection Surface vegetation monitoring for terrestrial storage. 	Data processing can be time consuming and high-resolution imagery may not be able to detect subtle features and variations based on study area. Soil gas data required to interpret CO ₂ concentration/flux results.
Passive Scanners (SEQURE™)	<ul style="list-style-type: none"> NETL 	Airborne-based platform used to detect CH ₄ and CO ₂ leaking from the subsurface.	<ul style="list-style-type: none"> Pipeline and underground leak detection Abandoned wellhead identification 	Scanner effectiveness can be limited by resolution, size of study area, and method of deployment. Short duration CO ₂ release may not be detectable. Requires determining background concentrations.

Figure 2.2 Remote sensing technologies funded by the US National Energy Technology Laboratory (NETL) (after Litynski et al. 2013)

2.1 In Salah CO₂ storage site, Algeria

A suite of monitoring techniques for In Salah CO₂ storage site were evaluated by In Salah JIP to assess the cost-to-benefit of each technology using the Boston Square method (Fig 2.3) (Mathieson et al. 2011). Fig. 2.3-left shows potential of the monitoring technologies before initial testing and Fig. 2.3-right shows their promise after initial testing. Note that satellite imaging is indicated in Fig. 2.3 as a key technology that has migrated from “consider as beneficial” in this domain, to a definite “just do it” (Eide 2012)". Geomechanics is also considered as a "just do it" tool since it locates in the lower left of the diagram with low cost and high benefit. The objective of SENSE is to integrate surface motion with geomechanics and thus increase the benefit of satellite imaging (move it downwards in the Boston diagram). Simultaneously, we intend to reduce the costs for satellite imaging through automatic processing schemes (move it towards left in the Boston diagram). SENSE will also increase the benefit of geomechanical monitoring through coupling the mechanics of storage complex to the hydro-dynamic events of reservoir, i.e. moving Geomechanics further down in the Boston Square (Fig. 2.3).

InSAR data acquired over Krechba, In Salah, have been very beneficial. They were the basis for multiple publications where researchers tried to understand the response of a naturally fractured and faulted reservoir to various injection rates, hydromechanics events that occurred in the reservoir due to injection operations, and the surface signature or faults and fracture zones in the subsurface (Vasco et al. 2008a, 2008b, Vasco and Ferreti 2008, Onuma and Ohkawa 2009, Rutqvist et al. 2009, Iding and Ringrose 2010, Vasco et al. 2010, Teatini et al. 2011, Cavanagh and Ringrose 2011, Deflandre et al. 2011, Ferreti et al. 2012, Goertz-Allmann et al. 2014, Oye et al. 2012, Rinaldi and Rutqvist 2013, Ringrose et al. 2013, Rucci et al. 2013, White et al. 2014, Jenkins et al. 2015, Bjørnarå et al. 2016, 2018, Bohlooli et al. 2017, 2018, Bui et al. 2018, Shi et al. 2012, 2013, 2019). There is still potential for further analysis of InSAR data from In Salah to understand longer term post-injection behaviour of the ground surface (and reservoir) following cessation of injection in 2011.

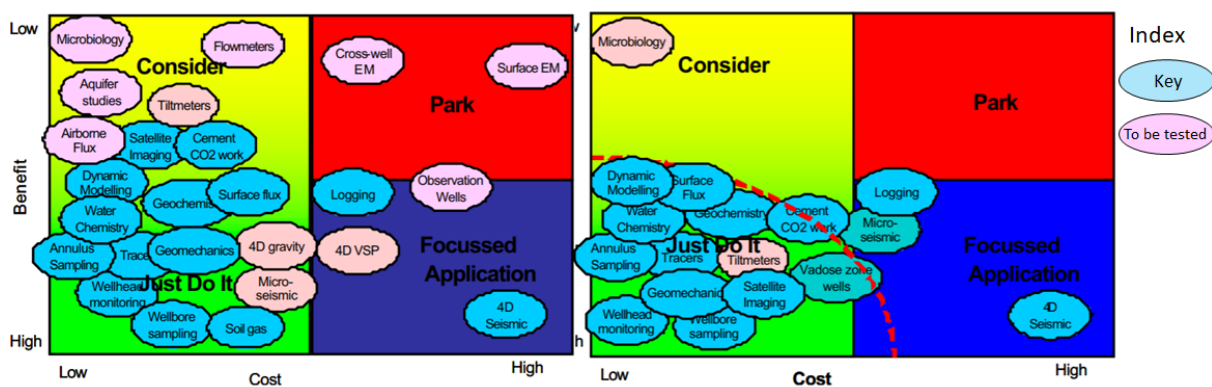


Figure 2.3 Evaluation of different methods for monitoring to CO₂ storage site at Krechba, In Salah before initial testing (left) and after initial testing (right) (modified after Mathieson et al. 2011 and Eide 2012).

2.2 Illinois Basin-Decatur Project, USA

The Illinois Basin-Decatur Project (IBDP) has injected about 1 million tons of carbon dioxide (CO₂) into a saline reservoir from November 2011 to November 2014. Carbon dioxide was captured from an ethanol production unit and injected into the Cambrian age Mt. Simon Sandstone (Freiburg et al. 2014) at a depth of about 2130 m below surface. The project was carried out by the Midwest

Geological Sequestration Consortium (MGSC) led by the Illinois State Geological Survey (ISGS) at the University of Illinois.

IBDP considered several tools for ground monitoring, among them is the aerial imagery, continuous GPS and InSAR data acquisition (Fig. 2.4). Aerial imagery data were planned to be acquired pre-injection, during injection and post-injection. However, GPS and InSAR data were planned to be acquired during the injection only (InSAR in 2011-2012 and GPS in 2012-2014). In order to improve the quality of satellite data 21 reflectors have been installed at surface close to the injection well (Fig. 2.4). Results from these measurements are not readily available yet.

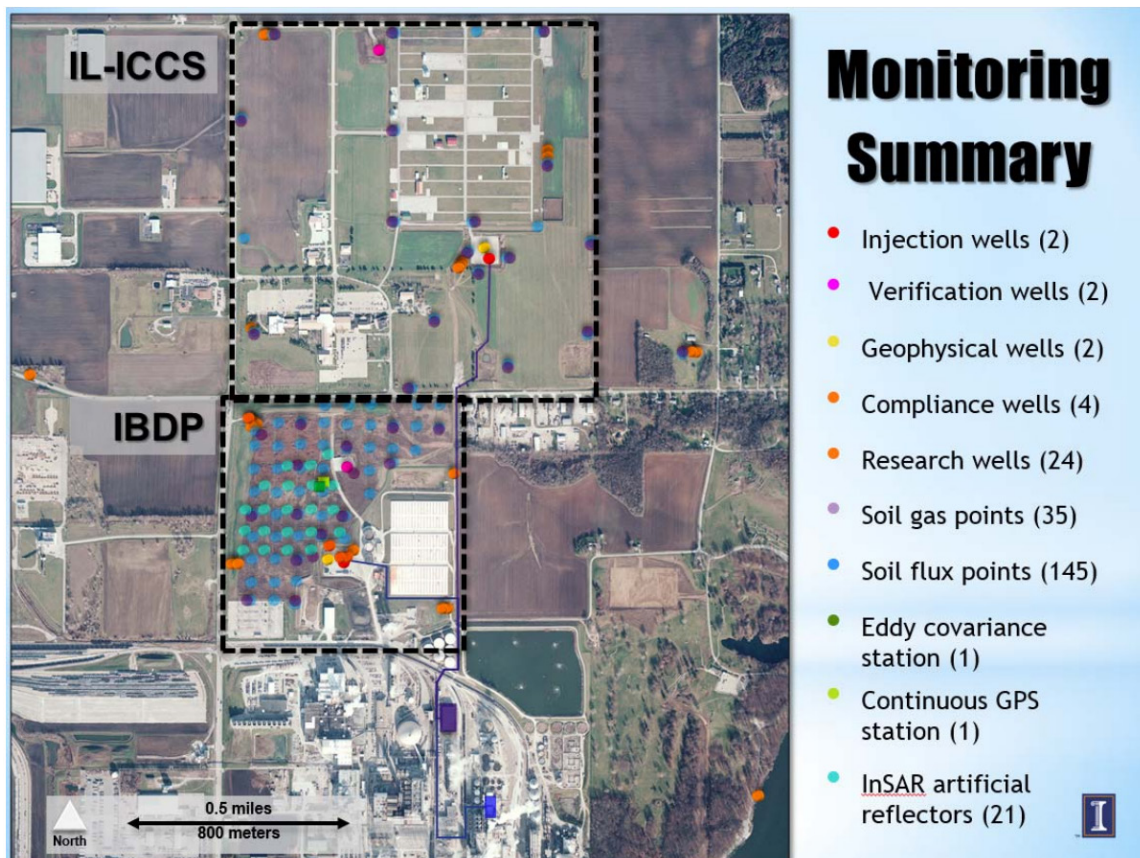


Figure 2.4 Monitoring plan for Illinois Basin Decatur Project, Illinois, USA (Locke 2017).

2.3 Quest Project, Canada

Quest project in Alberta, Canada (operated by Shell, Joint Venture: Shell, Chevron and Marathon) started storage of CO₂ into a saline aquifer from August 2015. The project captures more than one million tonnes of CO₂ per year from the Scotford oil sands bitumen upgrader located near Edmonton, Alberta. The captured CO₂ is injected into the Basal Cambrian age Sandstone, a deep saline aquifer located at a depth of about 2 km below ground surface, over a potential time period of 25 years. An important part of the QUEST project is its Measurement, Monitoring and Verification (MMV) plan to demonstrate containment and conformance of the injected CO₂ (Rock and O'Brien 2017). The MMV plan for Quest includes diverse methods as presented in Fig. 2.5. InSAR monitoring has been considered for Quest in all phases of the project; i.e. pre-injection (baseline), injection and post-injection (closure).

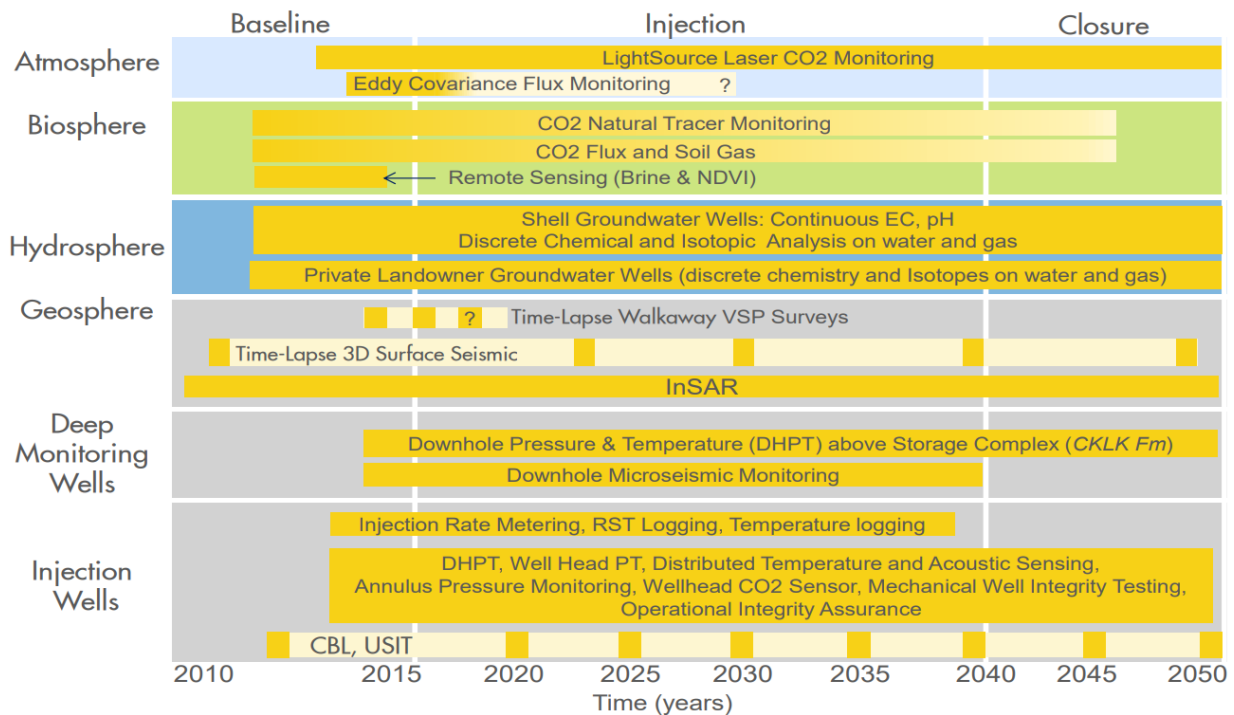


Figure 2.5 Measurement, Monitoring and Verification (MMV) plan for Quest CO2 storage site, Alberta, Canada (after Rock and O'Brien, 2016). InSAR is one of the monitoring methods planned throughout all project phases.

2.4 Sleipner CO2 storage, Norway

At the Sleipner CO2 storage site in the North Sea, 1 million tonnes of CO2 per year have been injected since 1996 into the Utsira formation, which is located at an approximate depth of 1000 m. To monitor the behaviour of the CO2 plume in time, 3D seismic surveys have been the key monitoring technique, used since 1994, which have provided the best resolution for studying CO2 plume migration. A varied time-lapse monitoring programme has been carried out at the Sleipner site to evaluate storage performance and integrity as well as to test out tools and to improve understanding of CO2 migration and trapping mechanisms in the storage reservoir (Fig. 2.6) (Zweigel et al. 2004, Eiken et al. 2011, Chadwick and Eiken 2013, Furre et al. 2017).

Monitoring technique	1994	1995	1996	1997	1998	1999	2000	2001	2002	2003	2004	2005	2006	2007	2008	2009	2010	2011	2012	2013
3D surface seismic	✓					✓		✓	✓		✓		✓		✓		✓		✓	
2D surface seismic (hi-res)													✓							
Seabed gravity									✓			✓				✓				✓
CSEM															✓					
Wellhead pressure	continuous																			
Seabed imaging (ss sonar, multibeam, pinger)													✓					✓	✓	✓
Sediment sampling				✓			✓			✓								✓	✓	✓
Water column sampling, bubble stream chemistry																		✓	✓	✓
Cumulative CO ₂ injected at survey (Mt)	0.00		injection starts			2.35	4.25	4.97(s) 5.19(g)		6.84	7.74	8.40			10.15(s) 10.38(e)	11.05	12.1			~14

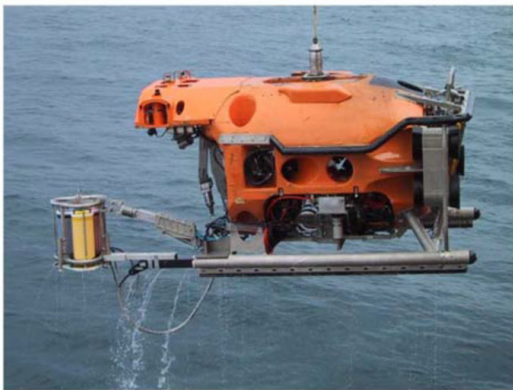
Figure 2.6 Monitoring methods deployed at Sleipner from 1994-2013 (after Hannis et al. 2017). For details see the reference).

Seabed gravimetry is another of the time-lapse MMV methods used at Sleipner. Gravity measurement gives an indication of the density change (CO2 plume migration in the subsurface). An initial seabed gravity survey was acquired at Sleipner in 2002 with 5.19 Mt of CO2 injected. Repeat

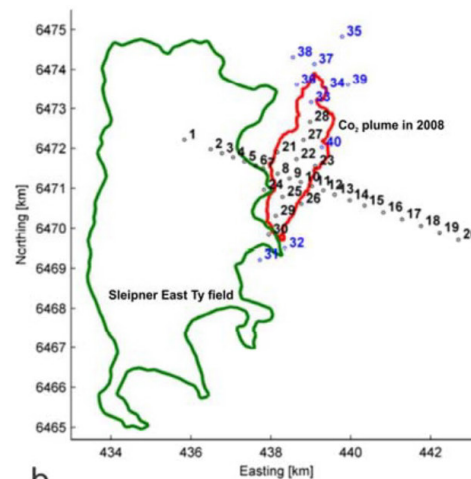
surveys were then acquired in 2005 and 2009 with 7.74 Mt and 11.05 Mt of CO₂ injected respectively. The surveys used pre-positioned concrete benchmarks on the seafloor that served as reference locations for the (repeated) gravity measurements. Relative gravity and water pressure readings were taken at each benchmark by a customised gravimetry and pressure measurement module mounted on a Remotely Operated Vehicle (Fig. 2.7).

Seabed imaging surveys (sidescan sonar, single beam and multibeam echosounding and pinger seabottom profiler) were also acquired at Sleipner in 2006 and 2011 - 2013. During the 2006 survey, a digital seabed bathymetry terrain model with 2m x 2m sampling was made from the multibeam echosounding showing the seafloor dipping gently from 80.8 m depth in the east to 83.0 m in the west.

Accurate vertical motion of seabed at Sleipner seems not been included in the monitoring plan. Such an accurate measurement will also be beneficial for gravimetry data as it will provide a reliable reference seabed level.



a



b

Figure 2.7 ROV and seabed gravimeter deployed at Sleipner (a) and layout of the seabed benchmarks (b) relative to the footprint of CO₂ plume in 2008 (after Chadwick and Eiken 2013).

2.5 Snøhvit CO₂ storage, Norway

Snøhvit presents a CO₂ storage case where natural gas is transported to land (Melkøya) and CO₂ is separated from the gas and captured onshore. The separated CO₂ is then transported back through a CO₂ pipeline of about 150 km long to Snøhvit where it is injected into saline aquifers c. 2.5 km deep, adjacent to gas field. Initially, CO₂ was stored in the Tubåen geological Formation. and then in the Stø geological formation (since 2011).

3D seismic and downhole instrumentation have been the major monitoring methods deployed at Snøhvit. However, gravimetry is also carried out over the field (Fig. 2.8). In 2019, a new gravimetry survey was deployed at Snøhvit by Octio Gravitude. "At the end of this year's survey at Snøhvit, Albatross and Askeladd, the repeatability has been measured to be 0.8 μ Gal and 2.2 mm respectively for gravity and depth data", announced Octio Gravitude (2019).

Monitoring technique	2003	2004	2005	2006	2007	2008	2009	2010	2011	2012	2013
3D surface seismic	✓						✓		✓	✓	
High resolution 3D seismic (p-cable)									✓		✓
Seabed gravity					✓				✓		
Downhole pressure						continuous					
Wellhead pressure						continuous					
Multibeam echosounding									✓		✓
Conductivity - temperature - depth profiles									✓		✓
Sediment sampling											✓
Water column sampling											✓
Cumulative CO ₂ injected (average, Mt)	0					injection starts	0.5		1.0		

Figure 2.8 Monitoring surveys deployed at Snøhvit from 2003 to 2013 (after Hannis et al. 2017)

In summary, radar interferometry (cf. Section 3) has been used or is currently in use for several large-scale onshore CO₂ storage sites including In Salah, Decatur and Quest. The benefit of these data for different sites will depend on the local geological conditions, surface conditions and injection operations. For In Salah, studies carried out by many research teams around the world have demonstrated the great value of such datasets for monitoring ground surface deformation and hence understanding geomechanical response of the storage complex to pressurization of the reservoir. For Decatur and Quest, InSAR data have not been released to the research community yet and therefore the benefit of the technology for these sites is not yet widely known.

Seabed monitoring from CO₂ storage sites is mainly limited to gravimetry at the two offshore CO₂ storage sites in the world, i.e. Sleipner and Snøhvit. There are benchmark blocks at sea bottom above the storage reservoirs at both locations. The benchmarks serve as stations for gravimetry and static pressure measurements. The focus of these measurements is on the determination of seafloor subsidence due to hydrocarbon production.

3. Satellite-based ground monitoring

InSAR, represents a microwave remote sensing technique that can be used to determine surface deformations in the line-of-sight (LOS) direction of a radar sensor, by pairing SAR images capturing the same location from the same position at different times. Differential SAR Interferometry (DInSAR) is a specific version of SAR data processing, where two radar images of the same location on the ground are differenced from each other and the topographic phase contribution is removed in order to separate out the phase information caused by radar path delays. This phase information, represented in an interferogram, is used to measure the ground displacement that has taken place between the two captured moments that make the interferogram (see Appendix A for more details).

DInSAR is ideal to measure displacements caused by sudden events like, e.g., earthquakes. The images for the InSAR pair are selected from before and after the event, with as little temporal separation as possible. This ensures a good coherence of the interferometric phase. For very slow movements, this technique is not sufficient. The time between acquisitions will either be too short to pick up enough displacement to be detectable, or the timespan will be too long to get a coherent interferometric phase. For these reasons, methods have been developed to process entire timeseries or stacks of SAR images, which allows for the detection and monitoring of comparably small terrain deformations (Figure 3.1). The most widely used methods are the Permanent Scatterer (PS) approach and the Small BAseline Subset (SBAS) approach.

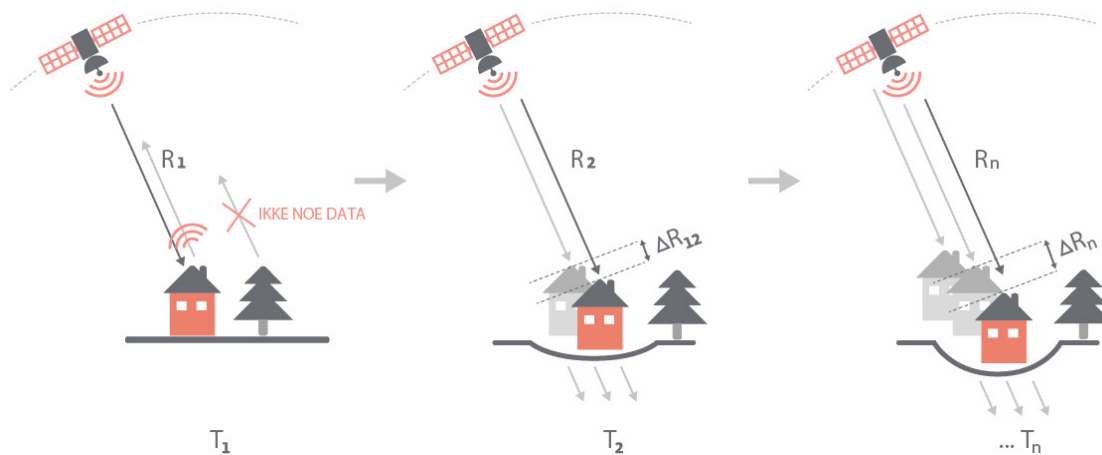


Figure 3.1 Observing continuous displacements with DInSAR. Modified based on Fig. 1 in Cespa et al. (2016).

3.1 SAR Interferometry in CO₂ storage applications

Ground displacements are an important parameter to observe during CO₂ injection. Injections are usually carried out over longer periods of time and, while displacement velocities are rather small, the expected uplift patterns can extend over many square kilometres. Hence, SAR interferometry has been identified as a potential technique to monitor (onshore) CO₂ injection operations. Eide (2012) reviewed several remote sensing techniques for their suitability for operational carbon capture and sequestration (CCS) monitoring. Among the studied remote sensing technologies *terrain motion monitoring by InSAR*, *direct and indirect use of hyperspectral technology*, and *gravity measurements* InSAR was deemed as the only technique mature enough for operational monitoring (Eide 2012).

The most prominent example of InSAR being applied to monitor surface deformation caused by CO₂ storage is In Salah field in Algeria. Vasco et al. (2008a) were among the first researchers to apply InSAR to a CO₂ storage site to map pressure changes at depth. Morris et al. (2011) applied InSAR within the In Salah project to determine injection induced mechanical deformation. The authors compared the deformations measured by InSAR with simulated uplift, including conducting and bounding faults to achieve agreement. Further, White et al. (2014) investigated the geomechanical behaviour of the reservoir and the caprock, by combining InSAR-based deformation measurements (Figure 3.2) with a number of ground-based measurements, including well logs, leak-off and formation integrity tests, core measurements, 3D and time-lapse seismic, water quality monitoring of the shallow aquifer, and surface gas monitoring.

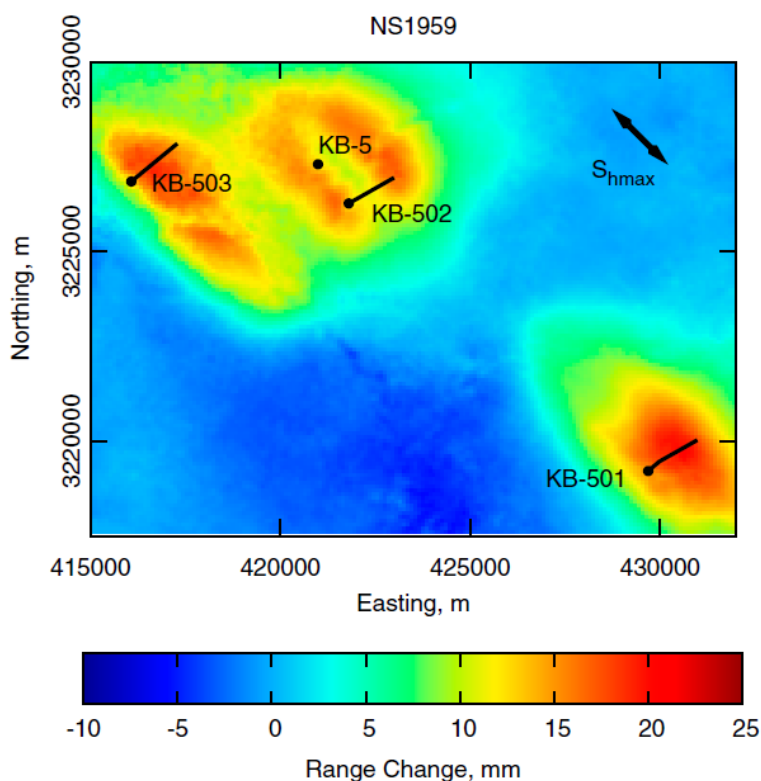


Figure 3.2 InSAR measured surface deformations at In Salah, as of March 2010 (after White et al. 2014).

While In Salah offers perfect conditions for InSAR, with no or very little vegetation in the entire area, Petrat et al. (2011) studied the applicability of InSAR at potential CO₂ storage sites in Europe, where much more challenging conditions are to be expected. Ground deformation was monitored at the Aquistore CO₂ storage site in Saskatchewan, Canada, which has a more vegetated surface. Worth et al. (2014) combined a range of remote sensing and ground-based methods to test and develop methods for effective monitoring of CO₂ storage sites, including a network of DGPS and tiltmeter stations. Kim and Lu (2018) studied the association between localized geohazards such as subsidence and micro-earthquakes and human activities, including CO₂ injection, in the Texas Permian Basin.

Zheng et al. (2019) have monitored surface displacements due to waste water injection into disposal wells. There exist also a number of studies not related to CO₂ injection or injection in general, but aiming at monitoring similar types of surface uplift, e.g. Colóna et al. (2016) monitored the variety of subaerial salt deformations using InSAR. Yang et al. (2019) used InSAR to map displacements in the Datong basin, which contains several faults and occurrences of fissures and areas with land subsidence of >20 mm/year, some of which related to coal mining areas.

In the past, NGI has applied InSAR to a range of geotechnical applications, including urban infrastructure monitoring, dam monitoring and landslide mapping. In these projects, both PS and SBAS processing techniques have been used, depending on the target site's scattering characteristics. Also, a range of satellites have been used in these projects, including Sentinel-1, Radarsat-2, TerraSAR-X, Envisat, ERS1/2 and ALOS Palsar. Figure 3.3 shows results from a study comparing three different InSAR stacks (Sentinel-1, Radarsat-2 and TerraSAR-X) with different spatial resolutions for the area surrounding Oslo Central Station, Norway.

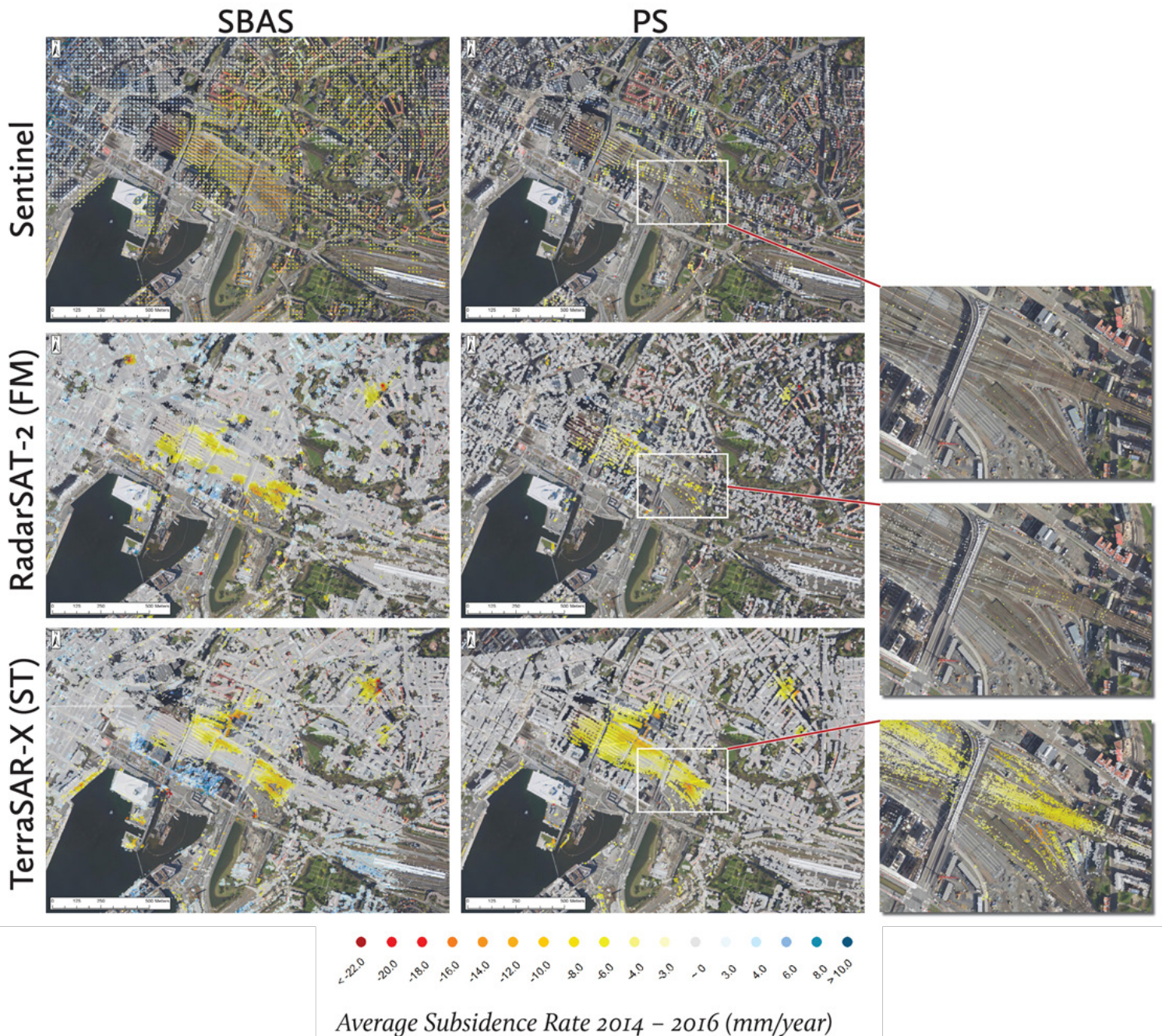
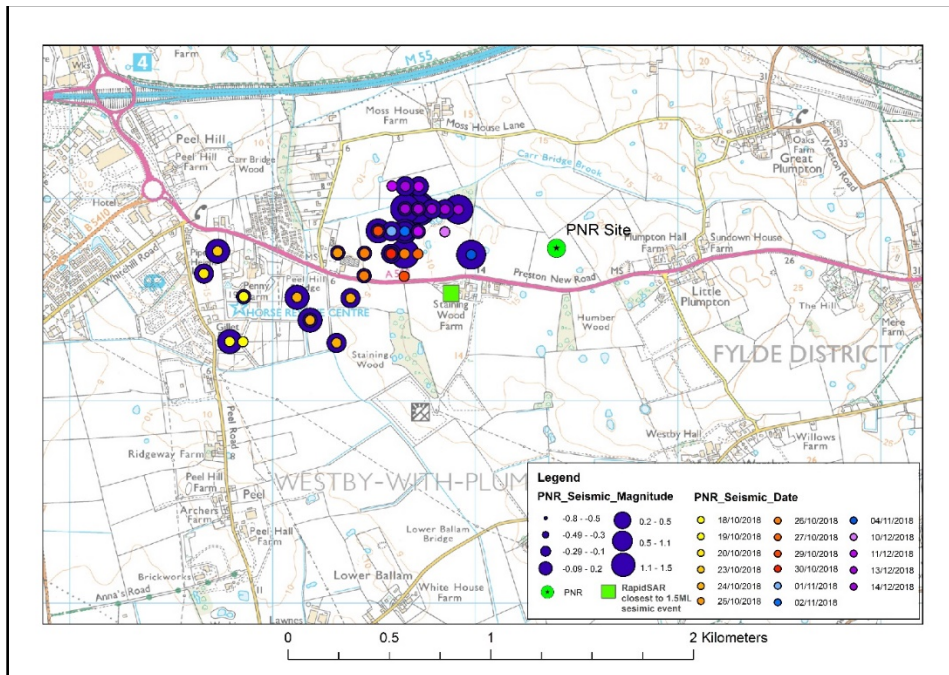
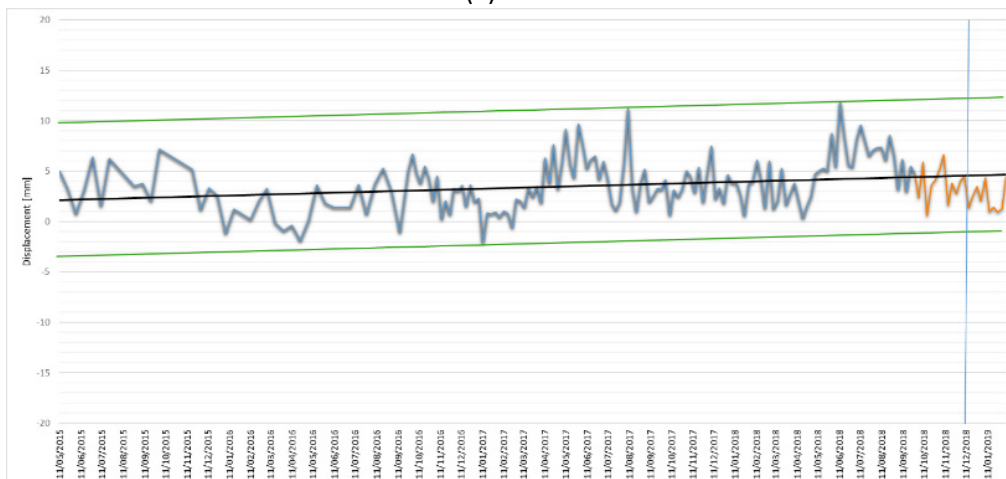


Figure 3.3 Comparison of InSAR results for PS and SBAS processing techniques for central Oslo, Norway. Subsidence over the area has been mapped using four different InSAR stacks with different resolutions: (upper row) Sentinel-1 (~10 m); Radarsat-2 Standard Mode (~16 m) (not shown); (middle row) Radarsat-2 Fine Mode (~7 m); (lower row) TerraSAR-X Staring Spotlight (~0,7 m). From late 2014 all four stacks cover the target area and a direct comparison of the different resolutions was possible. All stacks were processed with the SBAS workflow as well as with the PS workflow (see Section 3.2 and 3.3) using the SARscapeTM software. Satellite data sources: Sentinel: Copyright © Copernicus Sentinel data 2014-2016; Radarsat-2: Copyright © MDA/NSC/KSAT 2014-2016; TerraSAR-X: Copyright © 2014-2016 DLR, Distribution Airbus DS/Infoterra GmbH.

BGS have used InSAR to many applications and settings in the UK and overseas. UK projects have focused on monitoring of ground motions related to historical coal mining and the ground surface rebound as minewater pumps are turned off (Bateson et al. 2015., Gee et al. 2017., McCormack et al. 2013). The effect of ground water pumping in major cities (Boni et al. 2018) and the establishment of a ground motion environmental baseline for shale-gas and the monitoring of any changes brought about through hydraulic fracturing activities (Jordan et al. 2017, 2019). BGS are actively researching groundwater extraction related subsidence in Hanoi (Vietnam) and Bandung, (Indonesia) where an automatic processing chain is underway. In China slow moving landslides have been studied using SBAS techniques applied to ALOS PALSAR data (Zhang et al. 2018).



(a)



(b)

Figure 3.4 Preston New Road (PNR) shale-gas site showing location, date and magnitude of seismic events and location of the InSAR time series shown in the inset time series plot. The InSAR time series show no evidence of a change in ground motion at the time of the seismic activity compared to the preceding period. The graph on the right shows the time series for the pre hydraulic fracturing baseline

(blue line in time series plot) and the period when hydraulic fracturing took place (orange line). The black trend line shows the average motion whilst the green lines mark the maximum and minimum deviations from the mean. The blue vertical line marks the date of the strongest seismic event. InSAR continues to detect ground motion during the hydraulic fracturing period, and at the time of the seismic events, but the motion is no larger than the variation observed during the baseline period, and the trend of the average motion (i.e. uplift) is unchanged Contains Ordnance Data © Crown Copyright and database rights 2017, Seismic data © BEIS.

These studies have used both PS and SBAS based techniques to obtain the maximum number of accurate measurement points. Recently BGS have been investigating the use of passive corner reflectors on the UK landslide observatory on Hollin Hill in Yorkshire, a small, slow moving landslide on arable farm land.

3.2 The Persistent Scatterer technique (PS)

The interferometric phase is influenced by a series of parameters, such as the satellite-target relative position, temporal changes in the scene or atmospheric fluctuations. The Persistent Scatterer Technique was first proposed by Ferretti et al. (2001) to overcome the aforementioned limitations of DInSAR interferometry. The method is based on identifying stable reflectors in multi-temporal interferometric SAR scenes. The stable reflectors have been named Permanent (or persistent) scatterers and are exploited for obtaining millimetre crust deformations and improved digital elevation model accuracies (submeter level). Such persistent scatterers are natural or man-made objects that present a stable signal phase from an acquisition to another, displaying a high coherence over a SAR data stack. Ferretti et al. (2000, 2001) proposed an amplitude dispersion index for identifying these PS candidates, subsequently calling this approach "Persistent Scatterer interferometry", or in short: PSInSAR. More recently, to overcome the limits of PSInSAR, analysis of interferometric data-stacks is considering extracting displacement information not only from point-wise deterministic objects (i.e., PS), but also from distributed scatterers (DS) like in Ferretti et al. (2011).

3.3 The Small Baseline Subset technique (SBAS)

Since the above-mentioned index only can be applied for large data stacks, Berardino et al. (2002) proposed using a coherence stability indicator, which they call "Small Baseline Subset interferometry", in short: SBAS. The basic principle of this technique consists in finding a suitable combination of multiple interferograms with corresponding small baselines. The resulted small baseline interferograms are implemented in a linear model. By solving the linear model, the sampling rate of the method is increased, while phase noise is reduced, and backscatter preserved by choosing a coherence threshold. Like in the case of the PS method, only coherent pixels are exploited, but in the SBAS technique the values of the coherent pixels are interpolated over larger areas using Delaunay triangulation as described by Costantini and Rosen (1999).

Both techniques for the processing of interferometric stacks have been continuously developed over the past two decades and have reached a high level of maturity. Several open-source processing packages are available (e.g., SNAP, ROI_PAC, STAMPS, MintPy and Sarproz) that offer variants of the processing methods described above. Commercial software packages are also available, e.g., SARscape and GAMMA software.

3.4 Data

In addition to steadily improving processing methods and software, new satellites provide an increasing amount of data that are available for InSAR studies (Figure 3-5). Recent SAR satellites provide data that enable measurement of surface displacement with high temporal and spatial resolution over large areas. ESA's Sentinel-1 constellation (comprising two satellites, the first launched in 2014, the second in 2016) offers a high temporal resolution, with a revisit time of 6 days for the European continent, and up to 12 days in equatorial regions, with a spatial resolution of about 5 x 20 m. This is generally good enough to capture the uplift patterns expected from large scale CO₂ injection. Being designed for global monitoring, continuous InSAR image stacks are available from early 2015 for almost all landmasses worldwide. Sentinel-1 data are available free-of-charge. For targets requiring high spatial resolution, data from satellites like the German TerraSAR-X satellite are the best option. TerraSAR-X provides data with spatial resolutions down to 0.75 x 0.25 m. Using such data, even very small displacement patterns, can be monitored.

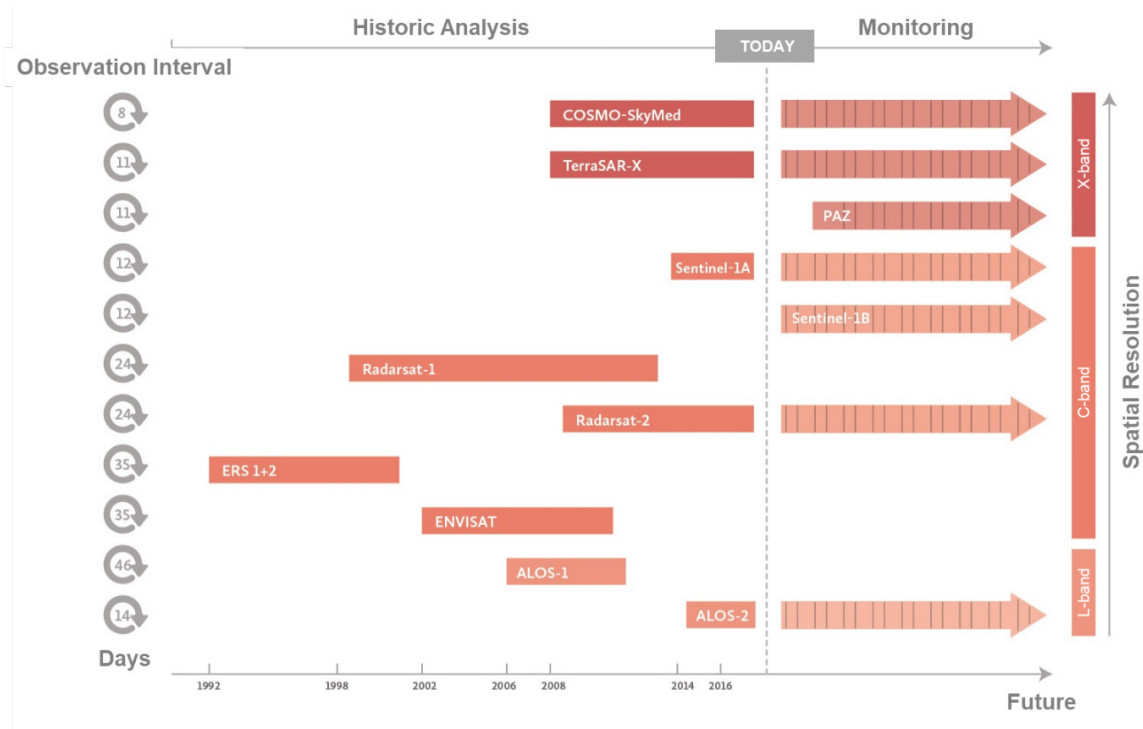


Figure 3-5: Available satellite constellations over the past 30 years (modified after TRE, 2019).

The choice of satellite within the SENSE project will be determined individually for each site, depending of each site's properties and the displacement patterns that are expected. Time series of at least 25 images are necessary to measure displacements in the mm range (see Appendix A for details). Due to ESA's free-data-access policy, Sentinel-1 data will be the primary choice in most cases. Since the expected ground deformations at the test sites will be of considerable size (several mm scale expected), Sentinel-1's special resolution should be sufficient for the task. Should the need for high resolution InSAR data arise, such data has to be ordered at least a year in advance of the CO₂ injection operation and obtained from commercial suppliers such as Airbus.

Sentinel-1's regular data acquisition (new data every 6 days in Europe), enables us to test near-real time radar data processing strategies to continuously monitor injection sites. Additionally, novel

statistical and geospatial data analysis techniques will be used to better interrogate the radar time series in order to detect anomalous changes in ground motion.

4. Seafloor deformation monitoring

Monitoring regulations and guidelines for CO₂ storage sites have been developed around the world during the past couple of decades. As the majority of mature offshore CO₂ storage sites (under operation and planned) are in Europe, the monitoring regulations have mainly been developed in Europe. Among these regulations are the requirements set by the EC Storage Directive which have been transposed into Member States regulatory frameworks and the OPSAR Convention. A review by Hannis et al. (2017) shows that two relatively consistent monitoring requirements have emerged: firstly, to demonstrate that a storage site is currently performing effectively and safely (containment assurance); and secondly to demonstrate (through the provision of information to support, and calibrate, predictions of future performance) that the site is reasonably expected to continue to behave as expected (conformance assurance). A third set of regulations may trigger additional monitoring (contingency) if the storage site does not meet the two main requirements mentioned above (Fig. 4.1).

Seafloor monitoring proposed in SENSE project will serve as a tool to assure storage containment through providing information on containment integrity. In addition, it can also detect the extent of uplifted areas and thus reveal migration of CO₂ in reservoir (Conformance). Seafloor monitoring combined with geomechanical modelling can be classified under the "Deep-focused" actions shown in Fig. 4.1.

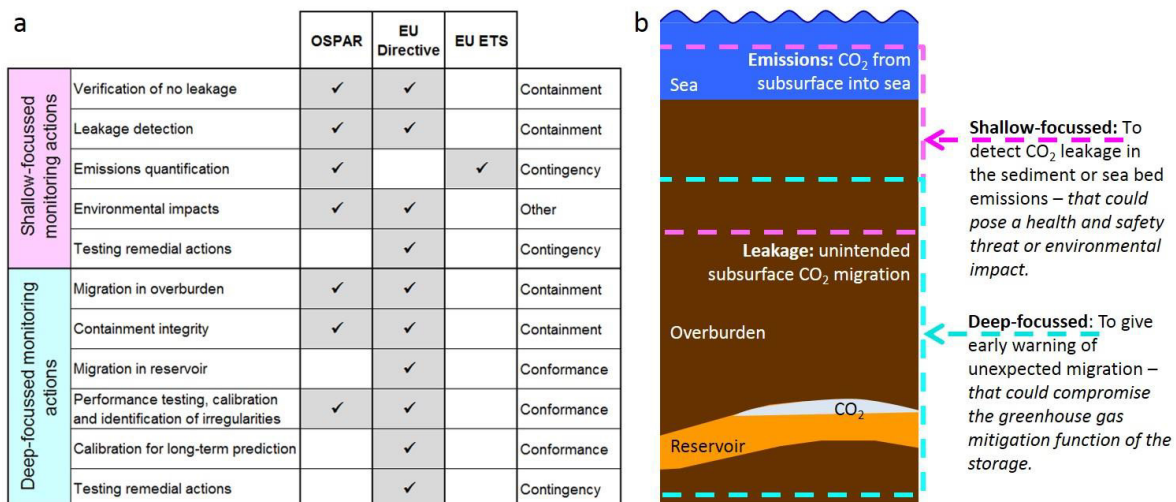


Figure 4.1 Key monitoring actions for offshore storage required under the European regulatory framework (a); and shallow and deep focused monitoring regimes (b) (After Hannis et al. 2017)

The state-of-the-art for seafloor monitoring mainly refers to existing technologies for subsidence monitoring due to reservoir compaction or slope creep movements (Hettema et al. 2002, Nooner et al. 2007, Chadwick and Eiken 2013, Eiken et al. 2011, Furre et al. 2015, 2017). The technology used for subsidence detection is, however, equally applicable to monitoring seafloor uplift due to pressure increase in a CO₂ storage context. Seafloor uplift caused by pressure increase due to fluid injection is illustrated in Fig. 4.7. The uplifted area may be surrounded by gentle slopes. Fractures/fissures may occur in the extension zones at the crest of the slopes, in case of stiff layers.

Signature of seafloor motion may be detected by periodic surveys using Remotely Operated Vehicles (ROV), sonar and seismic surveys. A challenge for monitoring seafloor level may be achieving effective coverage of the vast area being uplifted due to the pressurization of reservoir. Another issue is the slow and small deformations that may propagate to the seafloor which will mean that changes will be very slow and very small scale and therefore difficult to monitor with existing instruments.

Seafloor uplift caused by reservoir pressurisation can be characterised by an uplifted shape area with the highest points above the centre of the injection well, surrounded by gentle slopes. Vertical displacements at seafloor may be small, as measured for example for Troll Gas Field, and the gradient of the slopes may be less than 1:1000. Thus, sensing methods with high resolution and negligible instrument drift are required. It might be impractical to monitor the whole uplifted area (or subsided area in the case of fluid production) by direct measurements. Therefore, hot spots must be identified and selected for different types of instrumentation and measurements. To evaluate suitable monitoring strategies and most effective survey array, the expected reservoir-overburden expansion and subsequent uplift should be predicted using modelling. During the gravity surveys in 2002 and 2005 at the Sleipner, using fixed instruments, ground surface movement was also observed but the data were deemed unreliable due to scouring (removal of sediment from beneath the instrument stations), see e.g. Nooner et al. (2007).

As illustrated in Fig. 4.2, the following monitoring parameters/methodologies may be considered relevant for detecting vertical motion at seafloor:

a. Magnitude of motion/uplift

Magnitude of seafloor motion is normally determined from hydrostatic pressure measurements in the centre of the uplifted area (assumed to be subjected to the largest uplift compared to virgin seabed). The measurements must be compared to reference readings at stable seabed outside the uplifted area. In order to obtain the required precision, comprehensive statistical data processing is required to filter out natural pressure fluctuations caused by a changing water column above the sensor due to currents, density, tidal and atmospheric variations. In deep water, the necessity of having a large operational pressure range for pressure sensors means that extreme precision in the recorded data and sensor drift corrections during long-term monitoring are required. Alternatively, hydrostatic measurements can be performed as periodic survey campaigns deploying instruments on stable benchmarks which remain permanently on the seabed. Possible lateral deformations around an uplifted area are expected to be small and difficult to quantify across larger areas, unless specific anomalies or hot spots are identified (see paragraph c.). Such features can be detected by high-resolution microbathymetric surveys carried out by ROVs (Remotely Operated Vehicles) or AUVs (Autonomous Underwater Vehicles).

b. Changes in slope inclination around the crest of the uplifted area

Changes in slope inclination can be measured either by inclinometer chains across the slope or by tiltmeters in boreholes. Inclinometers have usually very high precision but provide point measurements only. Inclinometers require suitable mounting platforms, e.g. benchmark suction buckets, bed rock, or boreholes, providing a stiff and stable deep foundation that tilts with the seabed deformation. Scouring, dredging, trawling and geotechnical consolidation (settlement) must not affect the position of the benchmark.

c. Hot spots such as fractures and faults

If significant fissures or faults are identified by surveys, possible further deformations of these

"hot spots" (gap and relative strike and dip slips) may be effectively monitored. For small variations and local monitoring, direct extensometer measurement will provide the highest precision. For measurements across longer baselines (fissured zones), fibre-optic extensometers or acoustic ranging can provide information of the total extension of the seafloor between the measuring stations.

d. Microseismic events

Uplift/Subsidence and underground deformations may generate microseismic events that can be detected by seabed geophones. Detection of microseismic events will therefore provide additional information that can be correlated with the monitoring parameters listed above.

Registered microseismic events can also be used to trigger immediate recording of the other parameters listed above.

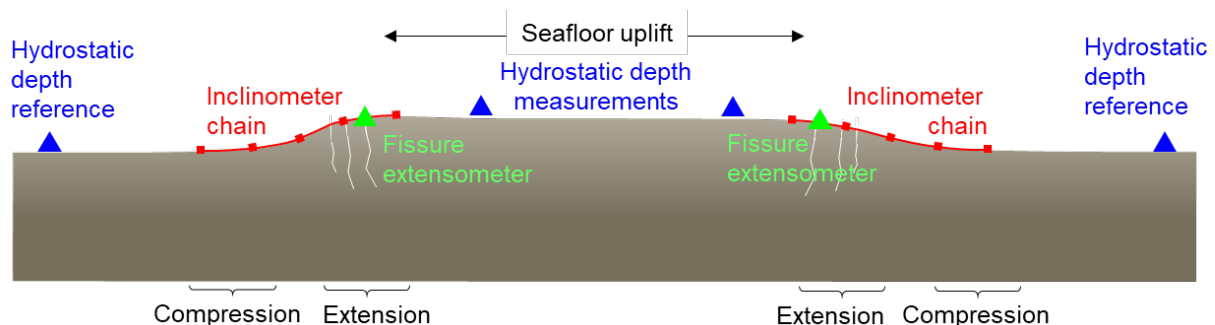


Figure 4.2 Definitions for seabed subsidence caused by reservoir compaction and possible monitoring methods. Note that the vertical scale is exaggerated.

Except for the survey methods, the monitoring arrangements described above relate to point or baseline measurements and the challenge is therefore to cover large areas with sufficient spatial resolution at a reasonable cost. Due to high cost of offshore operations, the location of sensors needs to be carefully considered and optimised. The data at the monitoring locations can be recorded on a periodic survey basis or by permanent monitoring stations (relevant for seismic recordings and probably tilt meters). A combination of survey and permanent monitoring is usually considered the best approach for CO₂ storage sites (see monitoring programmes at Sleipner, IBDP etc). Continuous monitoring of seabed deformation along the instrumented lines across the uplift area is another approach. For baseline profiling, distributed fibre optic strain sensing cables may be a promising solution for the future. Such a system is in use for monitoring ground deformations onshore but not yet applied subsea. In SENSE, within Work Package (WP) 2 and 3 we will select the optimal monitoring technology and validate it for offshore CO₂ storage sites.

4.2 Repeated bathymetric and seismic surveys

4.2.1 4.1.1 Bathymetric surveys

Most bathymetric surveys are acquired using multibeam echo sounder systems, which measure the seafloor depth using acoustic pulses emitted by a transducer array. Each signal pulse is directed in a specific angle from the ship by beamforming, which is the result of the superposition of multiple signals transmitted by separate transducers of the array. The emitted acoustic signal is scattered at the

seafloor and returns back to the vessel, where it is recorded by a receiver array. With information about the water sound velocity, the time between transmission and return of the signal constrains the water depth for a known transmission angle. By transmitting pulses along a swath of various angles, it is possible to measure the water depth beneath the vehicle in a stripe perpendicular to the ship's cruising direction, see Figure 4.3.

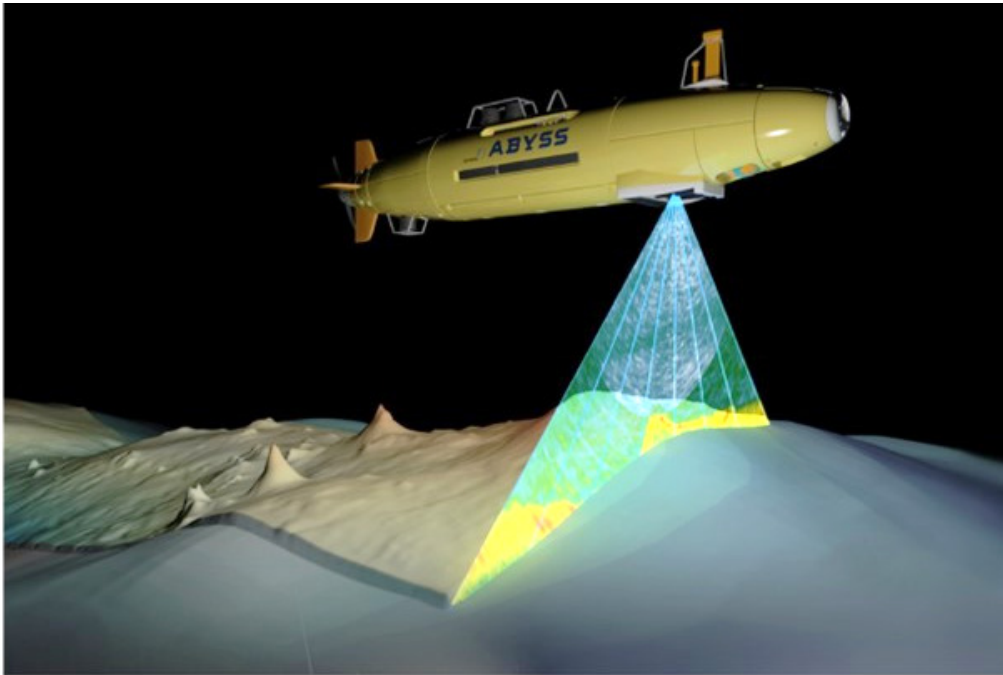


Figure 4.3 AUV-based bathymetry survey from (Wöfl et al. 2019).

The accuracy of multibeam echo sounder systems is controlled by their intended purpose and design. Systems for sounding deep waters are generally not capable of obtaining precise measurements in shallow water and vice-versa due to the survey specific amplitude and frequency of the emitted signal. Modern high-resolution shallow water multibeam systems may allow decimetre-scale horizontal resolutions and cm-scale vertical resolution. However, shallow water depth multibeam echo sounder are significantly more time-consuming than deep-water surveys due to the narrow swath width. The data quality and accuracy are generally controlled by the accuracy of the water sound velocity information, recordings of the ship motion (which need to be adjusted for precise beam-angle reconstruction), sea conditions and quality of information about weather and tide-controlled hydrologic variations. Bad weather conditions may significantly decrease data quality.

Ship-based multibeam surveys are a relatively cheap and fast method to acquire bathymetric grids. Multibeam echo sounder derived bathymetric grids generally have a high relative accuracy meaning that the relative depths within the survey are precise – down to centimetres for modern shallow water systems – however, the absolute accuracy of bathymetric surveys is generally poorer accuracy. Water column height changes due to weather and tides as well as variations in the water sound velocity profile may reduce the absolute accuracy significantly. The impact of these factors may be reduced by using Autonomous Underwater Vehicles (AUVs) for multibeam echo sounder surveying. However, the absolute accuracy of AUV-based bathymetric surveys is limited by the lack of direct positioning information (e.g. by GPS). In shallow waters (<80 m depending on visibility), it may be possible to apply LIDAR (light detection and ranging) using airborne platforms. The detection of

seafloor deformation with bathymetric surveys requires surveys with a relative accuracy greater than the deformation signal and information allowing absolute positioning of the measured grids.

Therefore, the feasibility of applying repeated multibeam echo sounder surveys for monitoring seafloor deformation depends on the amount expected deformation vs. the accuracy of measurements, which generally decreases with increasing water depth. The presence of reference points, for which an absolute position (and depth) is known (e.g. seafloor infrastructure), is reasonably expected to increase the absolute accuracy of bathymetric surveys.

There are several commercial companies offering multibeam echo sounder technology (e.g. Kongsberg, Teledyne, Reson, R2sonic, Norbit or Wärtsilä (former Elac Nautic), which provide a wide range of hull-mounted or mobile multibeam echo sounder systems for various purposes. All providers of AUV systems offer multibeam echo sounder systems for their platforms. Repeated bathymetric surveys have already been successfully applied for detecting large-scale seafloor changes (e.g. earthquakes or volcanic eruptions). In addition, this technique has been applied to determine ground deformation due to reservoir compaction (e.g. at the Dan field; Hatchel et al. 2007), see Figure 4.4

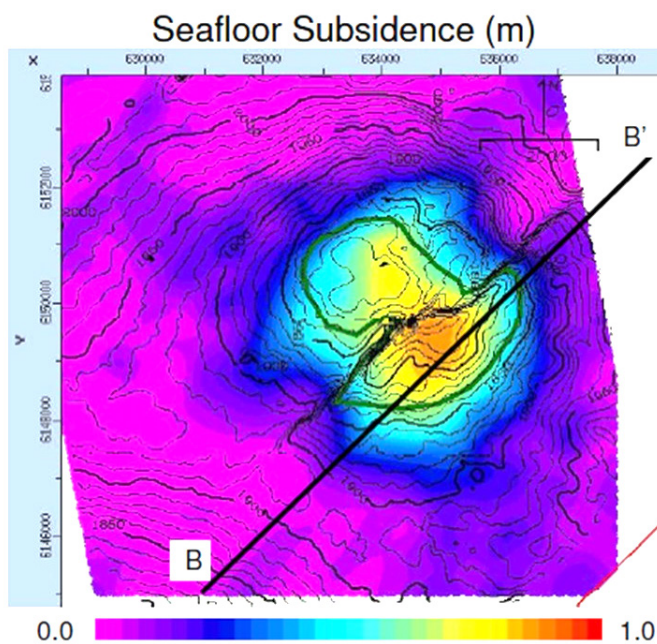


Figure 4.4 Seafloor subsidence due to production of the Dan gas field (from Hatchel et al. 2007).

As mentioned earlier the precision in bathymetric survey is not sufficient for monitoring gradual and small seabed deformations (centimetre scale) over larger areas but is useful a useful tool for detection of local anomalies such as pockmarks and cracks/faults that may have developed in the area.

4.2.2 Seismic surveys

Repeated 3D reflection seismic surveying (time-lapse seismic; 4D seismic) is the most common and precise technology for monitoring fluid migration in the subsurface. During reflection seismic surveys, an acoustic signal is emitted from a seismic source (most commonly an airgun at the sea surface) and travels to the seafloor, where a part of the signal is reflected back. A fraction of the

seismic energy penetrates into the seafloor and travels through the sediments or rocks and is again partly reflected at any boundary between rocks/sediments where acoustic properties of the layers change (more precisely at different seismic impedances, which is the product of density and seismic transmission velocity of the rock). The seismic signals from all subsurface reflections travel back to the sea surface, where they are recorded by seismic receivers (most commonly streamers in the marine realm). During 2D seismic acquisition a single streamer is generally towed behind the vessel (records a single line showing impedance changes along that profile), while during 3D seismic surveying (records a 3D block of data showing changes in impedance), multiple streamers are towed parallel behind the vessel, see Figure 4.5. Conventional industrial 3D seismic surveys generally have a horizontal resolution of 12.5 to 25 m. The vertical resolution of such datasets is generally >20 m, but depends on the frequency of the seismic signal (which depends on the seismic source) and the depth in the subsurface being studied (resolution decreases with depth) amongst other factors).

However, high-resolution 3D seismic systems (such as the P-Cable system) may acquire data with horizontal resolution of down to 3 m and vertical resolutions of <10 m. Ultra-high resolution systems like the Geochirp 3D system by (University of Southampton and Kongsberg) allow decimetre-scale horizontal and cm-scale vertical resolutions. However, such systems have a limited signal penetration (depth).

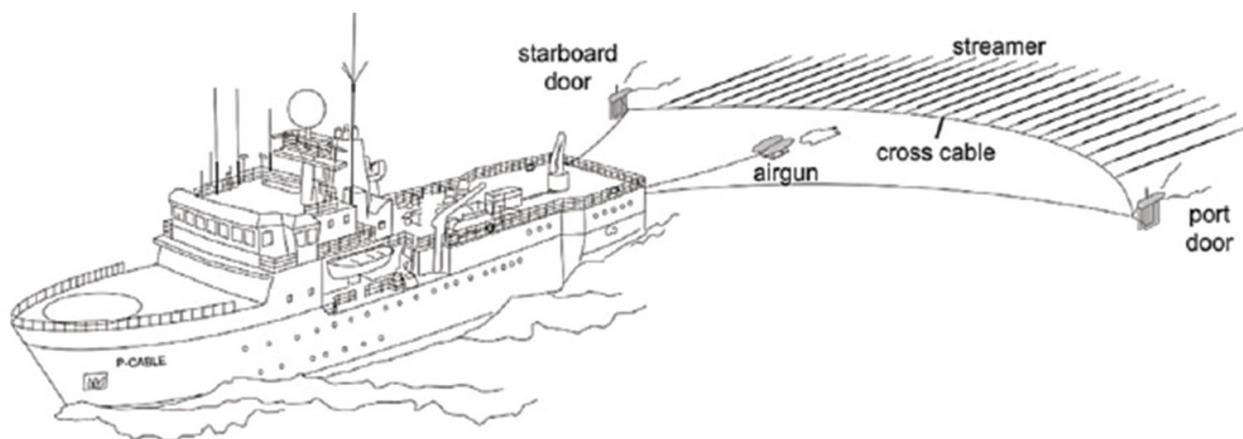


Figure 4.5 Sketch of the P-Cable System being towed behind a vessel (Petersen et al. 2010)

Repeated (time lapse) 3D seismic surveys have been completed in monitoring the two existing offshore CCS sites (Sleipner in the Norwegian North Sea and Snøvit in the Barents Sea - Furre et al., 2015, 2017; Karstens et al., 2017). At Sleipner, more than 18 Mt of CO₂ has been injected into the Utsira Formation since 2006 (Furre et al., 2017) and time lapse 3D seismic surveys allowed reconstruction of the growth of the CO₂ plume within the storage formation (Figure 4.6; Furre et al., 2017; Karstens et al., 2017).

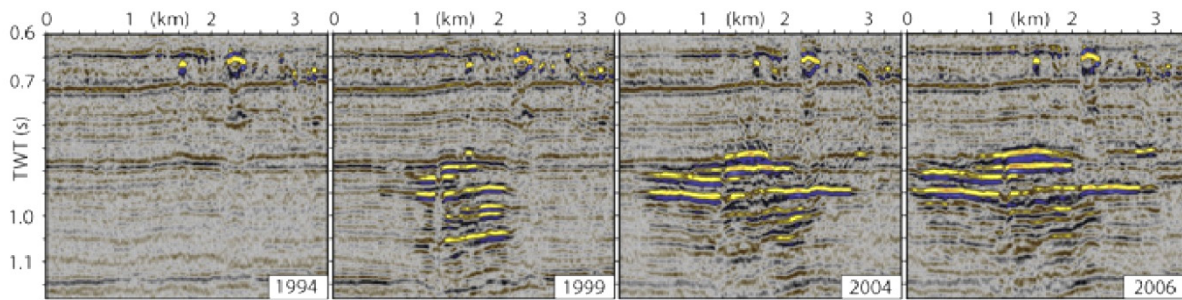


Figure 4.6 Timelapse 3D seismic at Sleipner reveals the growth of the CO₂ plume (Karstens et al., 2017).

4.3 Direct seabed deformation measurements

Depending on the area that needs to be monitored, the measuring points can be configured as single independent monitoring stations (Ocean Bottom Lander, OBL) or cable-based arrays (Ocean Bottom Cable, OBC). The OBL configuration is suitable when the distance between the monitoring points is large, OBL are fully autonomous units with self-contained power supply and data storage. Data is downloaded by recovery from the monitoring module at close range via data harvesting by inductive or LED modems or data transmission to the surface via an acoustic modem (high power demand). In deep waters, the OBLs may communicate with each other (seabed network) and the data are finally transmitted to the surface via one common link, for example, a telemetry buoy with inductive mooring.

A cable-based array (OBC) becomes attractive if monitoring is to be performed along a baseline (covering hot spots). The advantage of cabled arrays is that data from several monitoring points can be recorded at one common data acquisition point and power supply is much simpler. The unit cost for each monitoring point may then be decreased and data transmission/harvesting is performed at one location along the array. In many cases, for example, along the east coast of Japan and the west coast of Canada, the cabled arrays have communication and power cables to shore. The disadvantage might be the practical limitations in installation, coupling and recovery of cables and nodes. The end of the array (with data acquisition unit and power supplies) can consist of a larger seabed module if cabling to shore not is practical.

4.3.1 Long-distance acoustic direct-path long ranging network

Acoustic direct path ranging is a tool to detect relative distance changes between two/within a network of transponders (Spieß 1995, Bürgman & Chadwill 2014, Petersen et al. 2019). Such networks may be combined with interrogator units, which enable larger ranging distances and with satellite navigation, allowing absolute positioning of the transponder network (Figure 4.7, GPS-acoustic or GPS-A networks, Petersen et al. 2019). The transponders transmit a precisely timed acoustic signal, which is measured at the other stations.

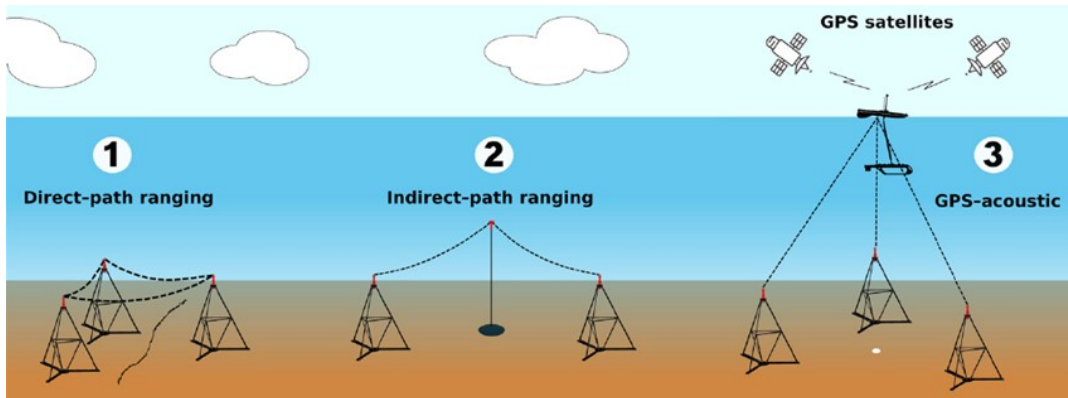


Figure 4.7 Conceptual acoustic direct-path ranging networks (from Petersen et al. 2019).

The time of flight (between signal transmission and receipt) can be transferred to distance with knowledge about the water sound velocity (Bürgman & Chadwill 2014), which is controlled by water temperature, salinity and pressure. These values may be measured by CTD-sensors (Conductivity, Temperature and Depth sensors) at the transponders. Acoustic ranging networks repeatedly communicate by sending acoustic signals, which are used to determine baseline ranges by long-term averaging. If the seafloor deforms the relative distance and thus the time of flight changes from the baseline measurements. The precision of such systems is controlled by the wavelength of the acoustic signal, the distance between the stations and the selected system. A recent analysis of multiple surveys in a range of water depths using the GEOMAR GeoSEA system revealed a baseline precision of 0.2 – 1.2 cm/km (Petersen et al. 2019).

Acoustic direct path ranging has been applied in various settings to measure seafloor deformation and strain built-up across faults, including the submerged flank of Mount Etna (Figure 4.8; Urlaub et al. 2018) and the North Anatolian Fault (Lange et al. 2019). In addition, this technique has been used in quantify strain changes and subsidence of Ormen Lange gas field in the Norwegian Sea (Dunn et al. 2016).

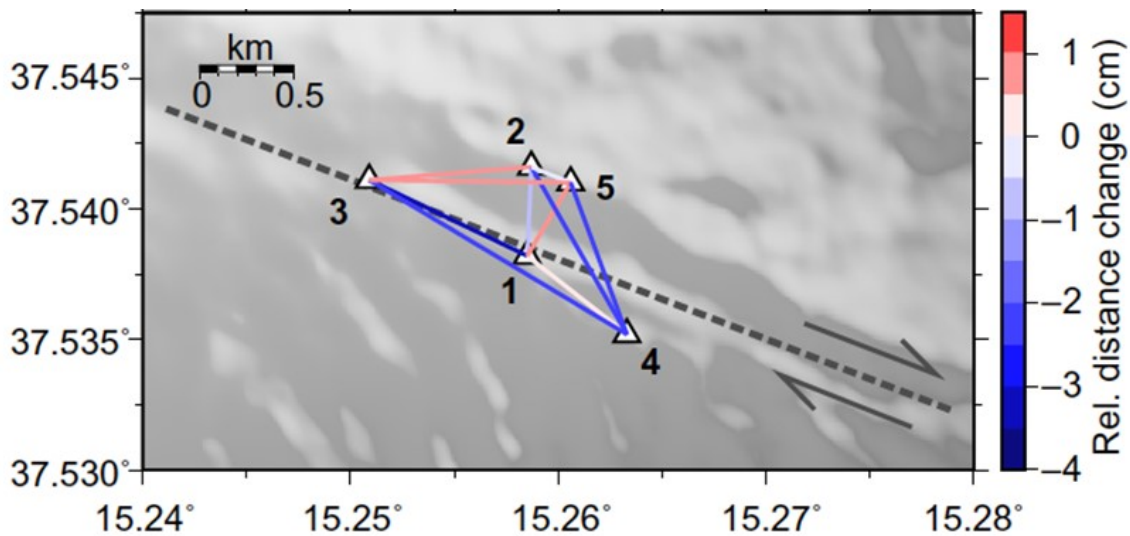


Figure 4.8 Displacement across a fault on the submerged flank of Mt. Etna measured with an acoustic direct path ranging network during 2017, from Urlaub et al. 2017

4.3.2 Short distance acoustic direct-path distance ranging networks

If significant faults or fissures are visible on the seabed (depends on sediment and site conditions) these features may indicate significant reservoir deformations and related deformations in the overburden.

The related seafloor deformation may be measured periodically based on ROV observations on graduated distance across the crack and line lasers. Such observations will only give limited information about crack development over time (dependent on time interval between surveys).

For a limited area (extension zone), high frequency sonar scanning of targets placed in the fissured area, can be used for continuous recordings of deformation across the fissured area, see Figure 4.9. The scanning sonar may also be used to detect gas bubbles migrating up from the cracks if they occur in sufficient density.

NGI have supplied a scanning sonar leakage detection system based on 6 sonar stations and methane sniffers. The system is the most extensive permanent leakage detection system installed to date and has been in operation beneath a North Sea platform complex for more than seven years.

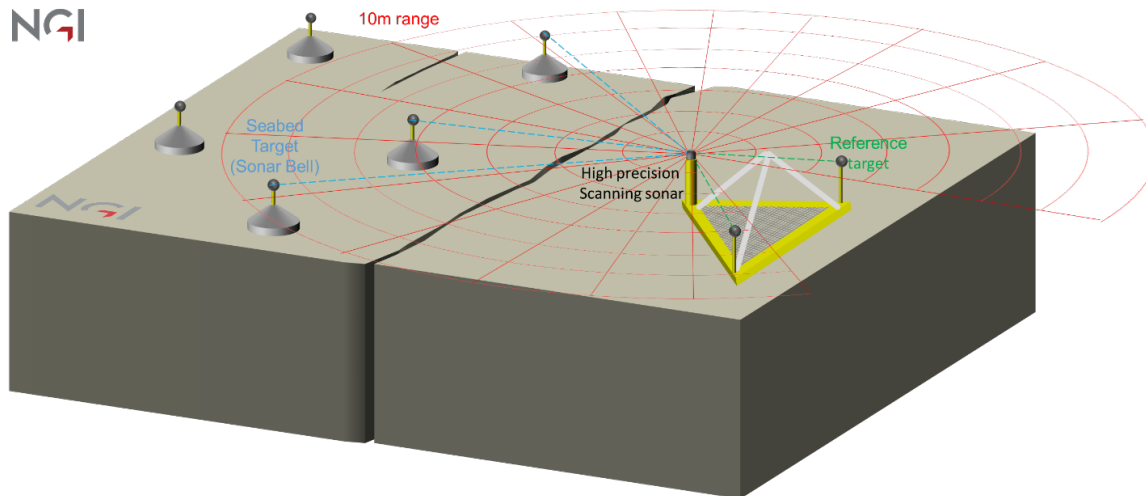


Figure 4.9 Arrangement proposed by NGI for monitoring horizontal deformations in a fissured area with a scanning sonar. The reference and fixed targets on the sonar platform are used to correct for variations of the speed of sound in the water between the periodic sonar scans

Identification and ranging of the sonar target can be automated, however development work is needed for embedded data processing of the acoustic signals in order to reduce the amount of data required to be stored or transmitted. Transmission of complete sonar images is demanding using acoustic modem due to the large file size. The resolution of this system is typically 0.5-5 mm but this is range dependent, for high frequency scanning sonars the maximum practical range is limited to ~75 m.

4.3.3 NGI Fault extensometers

For high precision measurements across specific cracks or faults, NGI propose to use customized extensometer systems. The fissure gap will be monitored with sub mm accuracy, strike and slip of the fault can be monitored if the pivot and rotation of the arm is recorded. Gap, strike and slip will be directly derived and logged as time-stamped values.

The NGI seabed fault recorder is used for local monitoring across a seabed crack/fissure with very high precision (an automatic extensometer). The distance between the anchor points can be up to 1.5 m (limited by ROV handling aspects).

The stroke sensor in the extensometer arm is used to monitor the gap across the crack and has following specifications:

- Extension Range: ~400 mm
- Linearity: 0.04% full stroke
- Repeatability: $< \pm 0.005\%$ of full stroke
- Resolution: < 0.01 mm (in practice dependent on background noise)

A uniaxial Micro-Electro-Mechanical Systems (MEMs) inclinometer is fitted into the sensor enclosure measuring changes in the vertical angle between the anchor blocks at each side of the crack (slip deformation):

- Range: $\pm 15^\circ$
- Full scale Linearity: 0.02°

- Resolution: 0.001° (relative slip <0.02 mm for 1m arm)

The submerged weight will be less than 50 kg allowing the unit to be carried and installed by ROV. Details for parking and ROV handling are to be discussed with ROV contractor and are not shown in Figure 4.10.

The unit can be operated as a standalone device with integrated data logger and battery pack or several units can be hooked up to a common seabed frame with jumper cables, DAQ and acoustic modems. Standalone seismic recorders may be placed in the fissured area for detection of micro seismic events from active cracks.

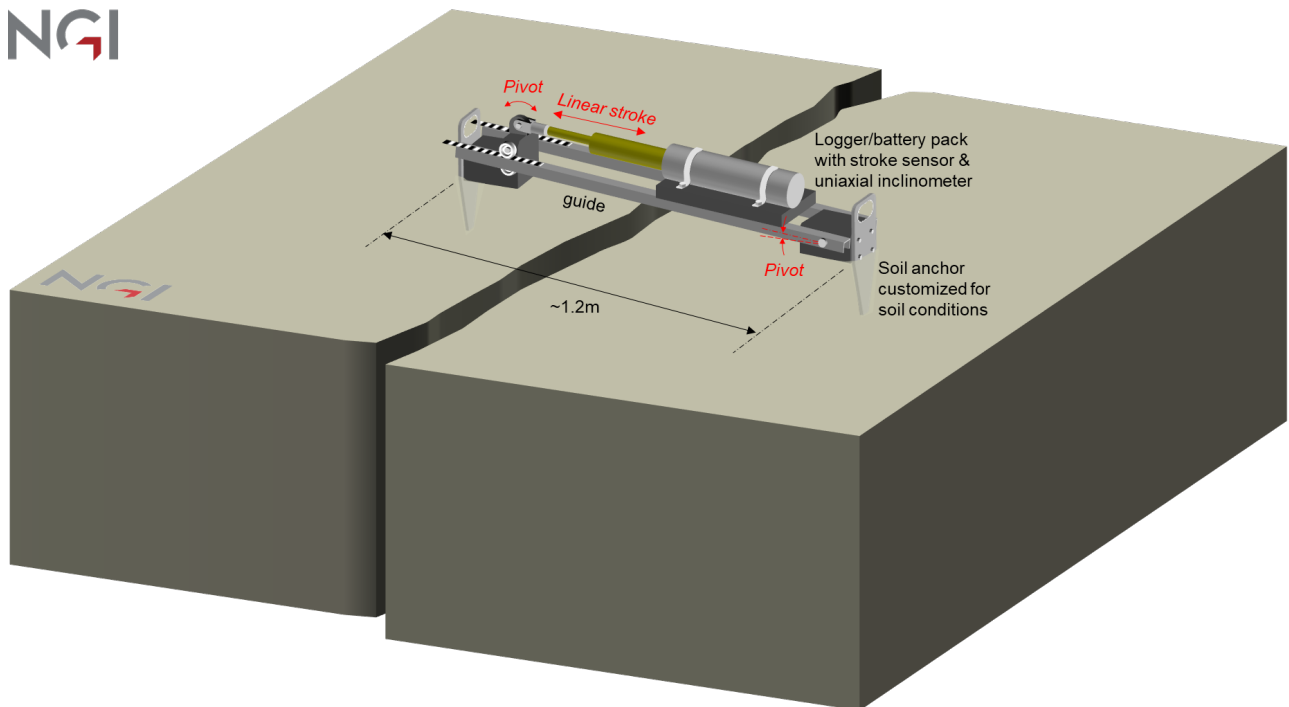


Figure 4.10 Outlines of NGI's seabed fault recorder

4.3.4 Seismic recorders

It is assumed that subsidence and surface deformation are generated by compaction and possibly failure of points within reservoir rock on a small scale and therefore a potential source of micro seismic events. Thus, monitoring micro seismic activity provides complementary information. Geophones or accelerometers can be combined with crack monitoring and or combined pressure and tilt recorders.

For optimum sensitivity and conformity to seabed seismic impedance, the geophone unit may be implanted directly in the seabed and hooked up to the main unit and DAQ system with a jumper cable. For simplicity and flexibility, standalone and standard OBS type of seismic recorders can also be used, see examples in Figure 4.11.

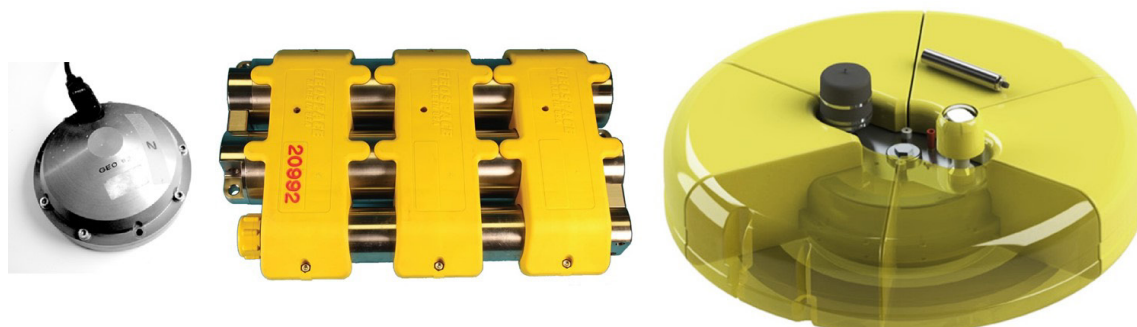


Figure 4.11 From left to right; 3C Geophone unit (must be hooked up to logger and power supply, Geospace OBX150 (150 days 4C recording capacity) and Guralp's Aquarius triaxial broadband seismometer with acoustic telemetry (18 months standalone recording capacity)

4.3.5 Ocean bottom pressure recorders

Ocean Bottom Pressure Recorders (OBPR) are normally used in tsunami warning systems but also for periodic or semi-permanent subsidence monitoring. The OBPR sensors measure the ambient pressure defined by the mass of the overlying water column, which allows the reconstruction of vertical seafloor deformation (Urlaub & Villinger 2018). The most commonly applied absolute pressure sensors in deep water are Paroscientific's Digiquartz Broadband sensors, which are used in most scientific long-term ocean-bottom pressure sensor networks (Polster et al. 2009). The sensors consist of a narrow and coiled metal tube and measure the coil's pressure-dependent deformation (uncoiling with increasing pressure), which results in strain variations sensed by an oscillating quartz element (Polster et al. 2009). For seabed subsidence or uplift monitoring the pressure readings are performed at stable seafloor benchmark positions above the reservoir subjected to compaction or uplift. In addition, reference benchmarks are positioned outside the subsidence/uplift area and used for calibration and compensation of sensor drift and hydrostatic variations in the water column (tide, barometric pressure, density, etc.). Benchmarks for subsidence and gravity monitoring have been installed at several gas fields in the North Sea and worldwide, e.g. Figure 4.12, these benchmarks are normally used for repeated surveys (Nooner et al. 2007, Eiken et al. 2011, Chadwick and Eiken 2013, van den Beukel et al. 2014, Furre et al. 2017, Vatshelle et al. 2017, Octio Gravitudo, 2019).

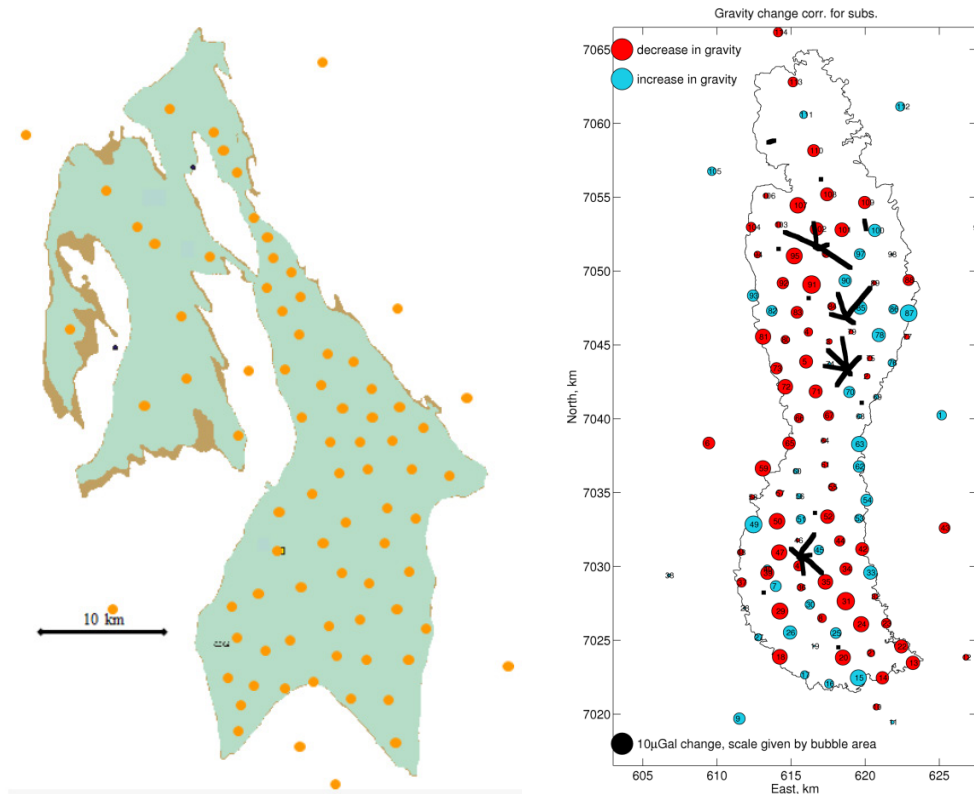


Figure 4.12 Map showing the footprint of the Troll gas field and the positions of the seafloor benchmarks permanently deployed for gravity/subsidence measurements (Quad Geometrics 2019), right: changes of gravity measured between 2012 and 2014 at Ormen Lange gas field (Octio 2019).

In other areas, for example along the continental slope outside the East coast of Japan and along the Cascadian subduction zone offshore the Canadian west coast, permanent OBPR's and seismic stations are installed in order to monitor subduction in conjunction with earthquakes, many of these stations are daisy chained in cable arrays (Fujimoto, 2013 and Seafloor Geodesy Cascadia Report, 2012). For long term deployment, drift of the pressure sensors may become an issue and some OBPR's are equipped with self-calibrating systems. Almost all OBPR's use as well as the Digiquartz pressure sensors from Paroscientific. Examples of different OBPR stations are shown in Figure 4.13.

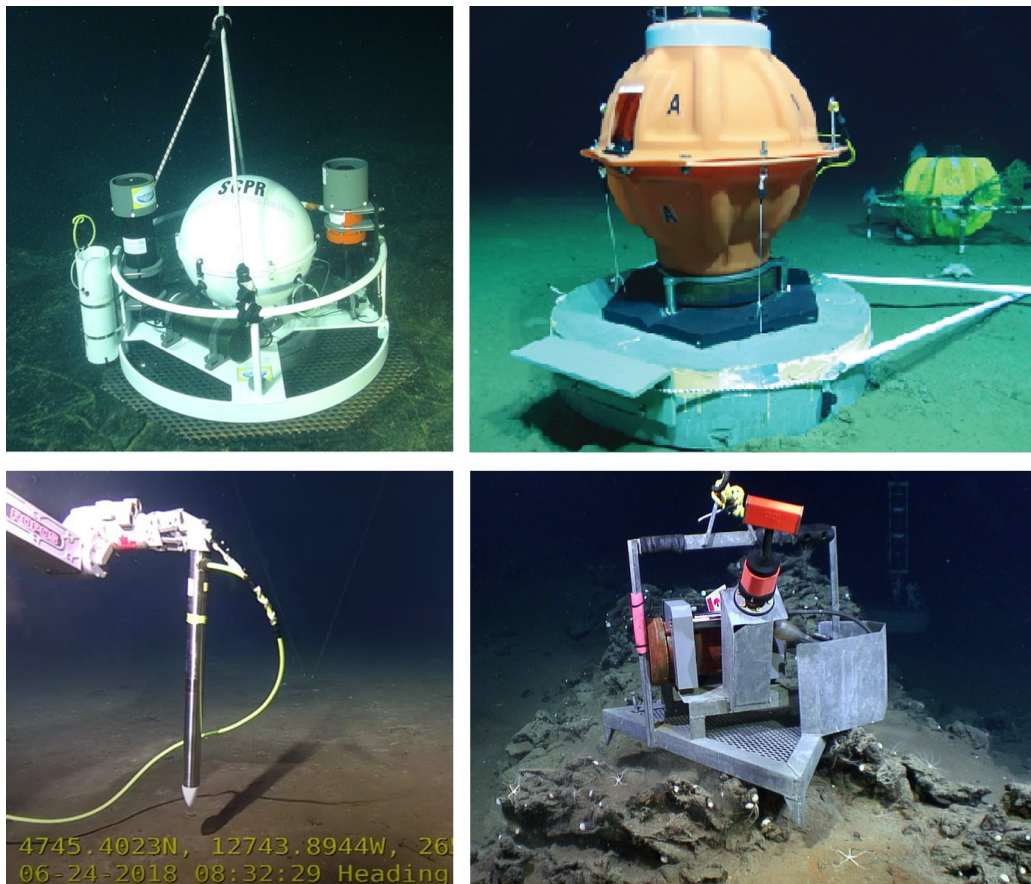


Figure 4.13 Examples of OBPR stations. Upper left and right: from Scripps and Sonardynes Fetch node, lower left: pressure recorder from RBR is implanted in the seabed. Lower right: shows an example of an unstable OBPR positioned on a rocky outcrop.

For long term deployment, drift in the pressure sensors may reduce the accuracy in hydrostatic depth measurements, therefore self-calibrating facilities have been implemented in state of the art OBPR stations. Scripps Institute uses an integrated dead weight tester (Sasagawa and Zumberge 2013). Paroscientific calibrates the hydrostatic pressure sensor against an internal barometer in their Seismic Oceanic Sensor (SOS) module (Paros and Kobayasi 2018).

gravity base foundation may also work if scouring is not an issue. Down-hole (well) applications are also relevant but have not been evaluated further in this study due to the relatively high cost of installation.

With respect to the biaxial (X-Y) inclinometer, the most important sensor performance indicators are long term stability (drift) and resolution. The linearity is not important as only very small changes in tilt are expected after installation. Unless the sensor has a self-levelling mechanism, a reasonable adjustment range is normally required in order to ensure that the instrument is within range after seabed installation. The most accurate tilt meters for geophysical monitoring are optical pendulum or bubble inclinometers, see examples in Figure 4.16. It should be noted that the sensor precision should be considered in light of site and installation conditions (background noise and benchmark stability will ultimately limit the quality of the data).

Recommended geophysical biaxial inclinometer specifications:

Range: min. +/- 10° or self levelling

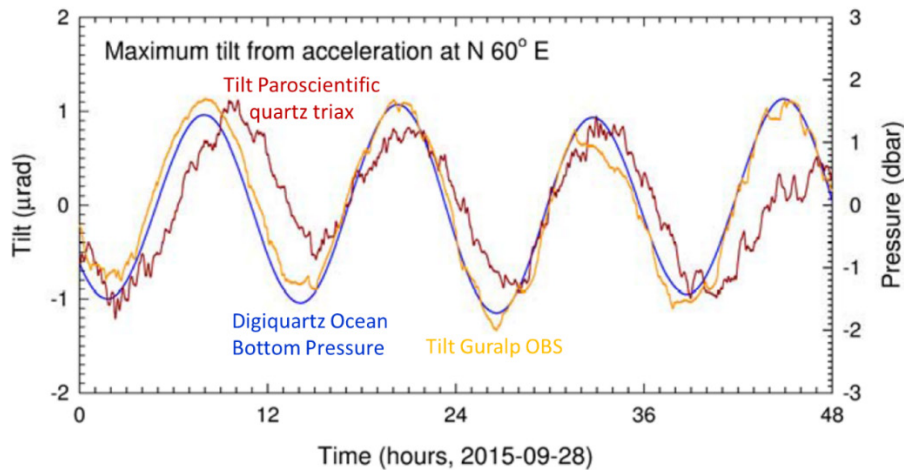
Resolution: Between 1nrad to 1μrad (depends on site and installation conditions)



Figure 4.16 Precision downhole inclinometers from Pinnacle (Halliburton) and Jewel instruments usually installed to monitor fracking. Right: Optical pendulum type of inclinometer from Scripps

Alternatively, the Triax quartz accelerometers included in the SOS module from Paroscientific can be used for tilt monitoring (in addition to seismic events), an example of data collected showing both ocean tide (ocean bottom pressure) and earth tide (max tilt) variations is illustrated in Figure 4.17. The tilt resolution is $\sim 0.03\mu\text{rad}$ and comparable with the high precision inclinometers described above. Paroscientific are currently testing out a dedicated quartz inclinometer with even better precision.

By means of the three X, Y and Z accelerometers, the in-place orientation is automatically determined relative to Earth's 1G gravity field. This allows for accurate measurements of tilt on each axis without a levelling system. Nano-resolution processing electronics provide parts-per-billion



resolution to make sensitive pressure measurements corresponding to fractions of a mm at depths of thousands of meters and acceleration measurements on a scale of nano-g's with 3G full-scale accelerometers.

Figure 4.17 Comparison of sea tide measured with digiquartz BPR and earth tide (seabed tilt variations) measured with Paroscientific's Quartz triax accelerometers and Guralp's OBS. The recordings were made in 2015 at Ocean Network Canada's Neptune seafloor observatory (1250 m water depth).

4.3.7 Benchmark foundations

Fixed seabed benchmarks provide a permanent and stable foundation for measurements over many years. The long-term displacement of the benchmark will follow the deformation of the seabed that is caused by reservoir expansion and seafloor uplift. The benchmarks shall not be subjected to local effects in the shallow sediments such as consolidation settlements and scour. The instrument package on top of the benchmark will be accessible for replacement by ROV and the interface shall allow for multipurpose use and precision docking of monitoring equipment. Benchmarks are typically used for gravity measurements, acoustic ranging, and ocean bottom pressure and tilt recorders.

For stable and firm seabed conditions gravity foundations (concrete blocks) can be used as benchmarks, see examples in Figure 4.18.



Figure 4.18 From left to right 1) Concrete benchmarks used by Quadgeo for gravimetric surveys, 2) Sonardynes FETCH instrument node on concrete benchmark deployed by Scripps for monitoring tectonic motion in the Cascadian subduction zone (photo David Chadwell) and 3) Concrete foundation block for Kongsberg's K-lander

For seafloor conditions with uneven surface, soft sediments or sand subjected to scouring, small suction piles can be suitable as benchmarks. Suction pile foundations with different geometries can be used for a large range of seabed conditions, see Figure 4.19. The suction pile is driven into the seabed by means of the hydraulic force (suction pressure) generated when water is pumped out from the confined void inside the pile. The foundation is unloaded when the pumping and suction pressure is aborted after completed penetration. Thus, a relatively deep and stable yet lightweight foundation is obtained. The suction pile can easily be extracted from the seabed by reversing the pump flow, i.e. jacking out the foundation from the seabed by over pressure.

Suction piles in various shapes and size is a well proven foundation concept within the offshore industry. The required outfitting, a 4" vent/pump inlet and the precise docking interface to the instrument unit (three male stabs) is indicated in Figure 4.19. The inlet shall be open during deployment to allow for air venting when the suction pile is submerged and for free water evacuation during landing and weight penetration. For optimal holding capacity, the pump inlet is closed and protected by a blind plug after completed installation.

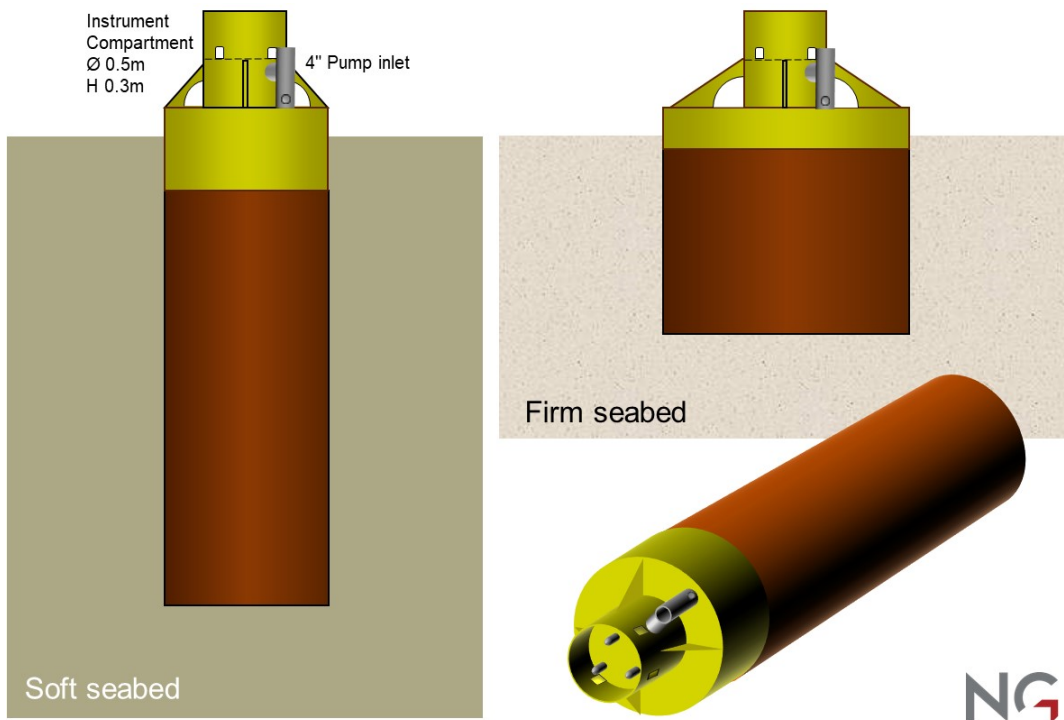


Figure 4.19 Outlines of suction anchor benchmark and outfitting proposed by NGI, the diameter may vary from 1-2 meter and embedment depth from 1-3m, dependent on soil conditions in field.

For small suction piles, a moderate capacity and small ROV pump can be used, see example in Figure 4.20. Such pumps are available for rental and most of the major ROV contractors possess such equipment in their tooling arsenal. The seabed installation can normally be completed within 1-2 hours. The duration of suction penetration phase is only 10-15 minutes. A bullseye indicator is recommended at the top to control that the verticality of the suction pile is well within the tolerances ($\pm 10^\circ$) for the instrument unit during installation.

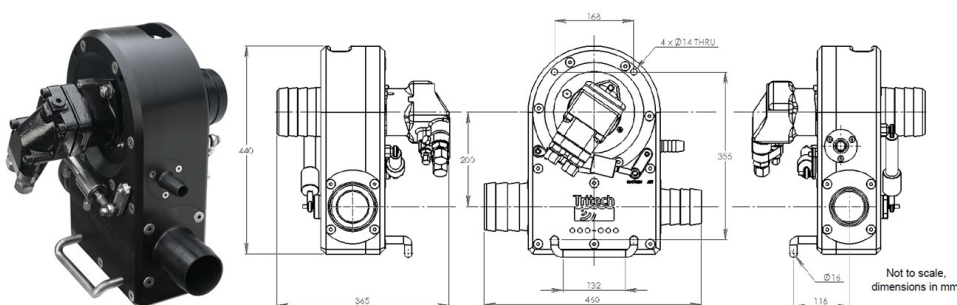


Figure 4.20 Super Zipjet pump by Trittech, flow capacity 30-50 m³/hr and submerged weight 11 kg

4.3.8 Seabed profiling using closed circuit liquid pressure systems

In geotechnical applications, different sensing solutions are used for deformation monitoring along sections of the ground (settlement profiling). The most common approach is the use of hydraulic settlement gauges, i.e. measuring the liquid head difference at different locations along a hydraulic tube. For subsea application, the hydraulic circuit must be closed to sea and a gas filled reference or compensating line must be added to the system to ensure that the reference pressure at each

measuring point along the liquid line is identical. The hydraulic and compensating (reference pressure) lines are terminated in a closed reservoir at the end (highest point) of the line with a gas/liquid interface. By means of a closed circuit the system is isolated from fluctuating pressures in the sea water column (tidal, waves, currents, density and barometric variations), the closed reservoir also compensates for volume changes in the system.

NGI has extensive experience of operating such systems and has developed closed loop liquid pressure systems for underwater applications (levelling). This type of system is however not practically feasible for long arrays and deep-water applications.

Agisco (2019) proposes a solution to the issue of volumetric changes in the sealed hydraulic lines by means of using a compensator instead of a reservoir. Thus, the system can be incorporated in a cabled array, see Figure 4.21. However, many practical aspects, such as excess pressure on the nodes when the cable hangs vertically during deep water deployment and long-term stability aspects, still need to be resolved. The depth rating is presently only 100 m and is limited by the liquid head acting on the deepest node during deployment.



Figure 4.21 Closed loop liquid pressure subsidence profiler (after Agisco 2019)

4.3.9 Baseline profiling using fibre optic strain cables

Fully distributed fiber optic sensing cables are used to measure ground deformation across long onshore lines and construction projects (slopes, embankments, bridges, dams, railways, pipelines, etc.). By means of scattered light of certain wavelengths along the fiber optic cable, temperature and strain can be determined along very long distances with high spatial resolution utilizing an interrogator hooked up to the cable. The scattered signals are sensitive to temperature and/or strain. Distributed fiber optic sensing systems are normally based on Rayleigh, Brillouin or Raman backscattering concepts, see Figure 4.22.

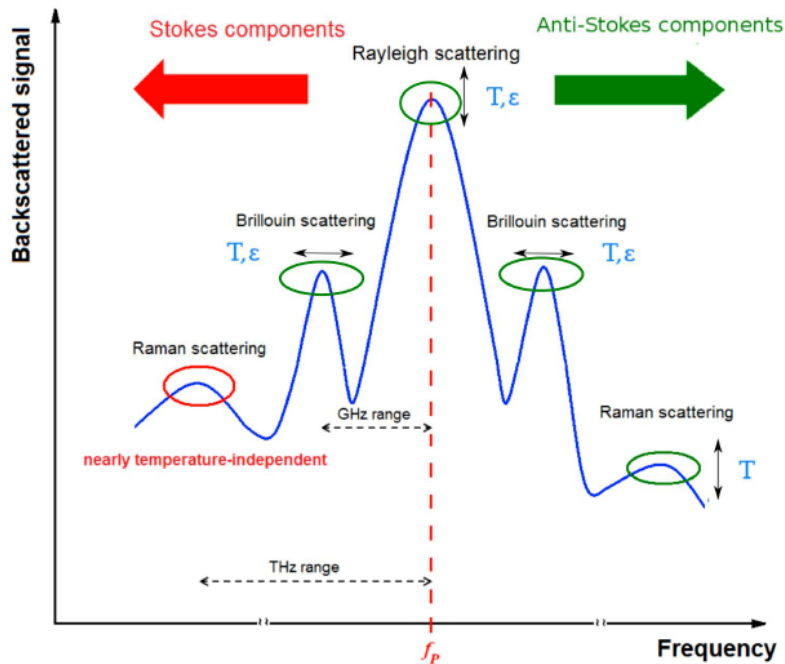


Figure 4.22 Different types of backscattering light in an optical fibre (Hicke 2018)

Rayleigh is the strongest backscattered signal and the intensity of the backscatter is sensitive for strain and temperature variations along the fibre. The sensing range is very long (fibre can be > 100 km) with a spatial resolution down to 1 m. The strain resolution is very high (nanostrain level) at fast sampling rates. Thus, the technology is suitable for Distributed Acoustic/Vibration Sensing (DAS/DVS), i.e. dynamic strain amplitude measurements comparable with hydrophones and geophones.

The spatial resolution of frequency shifts in the **Brillouin** backscatter varies linearly with temperature and strain in the fibre, see Figure 4.23. The sensing range is normally up to 50 km with a spatial resolution down to 0.1 m (depends on cable length) and a readout resolution of $\sim 2 \mu\epsilon$ (microstrain). Measurements from a strain relaxed fibre is used to compensate for temperature effects. The time for a complete reading scan depends on cable length and amount of measuring points from minutes to hours, thus suitable for static measurements.

The frequency changes from **Raman** backscatter are only sensitive to temperature variations and therefore are not applicable to DAS/DVS.

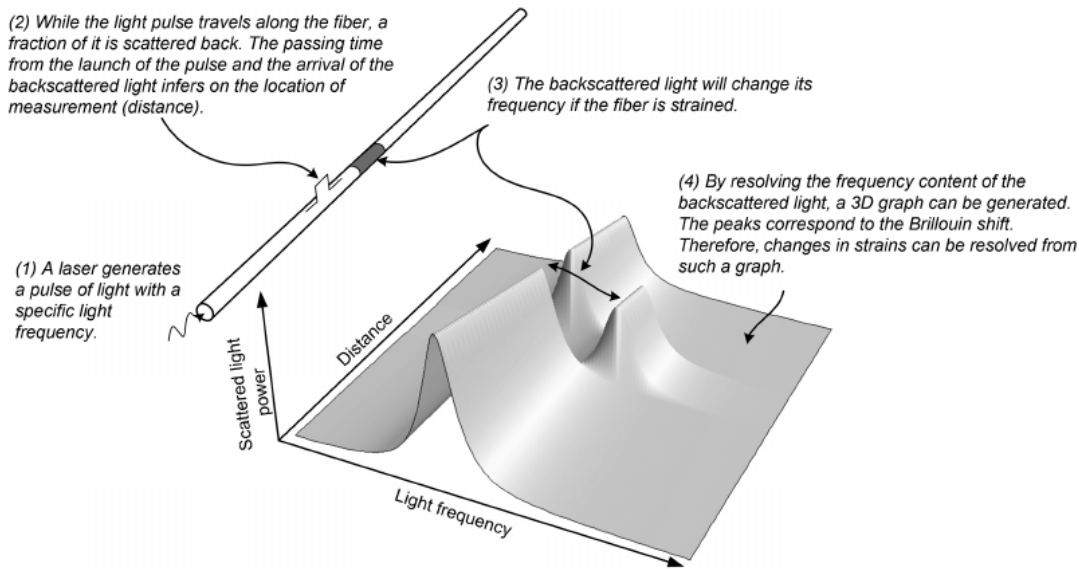


Figure 4.23 Principles for distributed strain measurements based on Brillouin scattering (Goldfeld and Klar 2013)

Presently the most common solution for distributed sensing of ground deformation is based on the Brillouin optical time-domain reflectometry or analysis (BOTDR/A) providing distributed measurements of strain along tens of kilometers of conventional optical fibres. If the bending direction or elongation of the cable is known (such as for settlement or subsidence), it is sufficient to record and integrate strain (or fibre elongation) along one fibre in the cable in addition to temperature compensating recordings (a DITEST Distributed TEMperature & STRain system), see example in Figure 4.24.

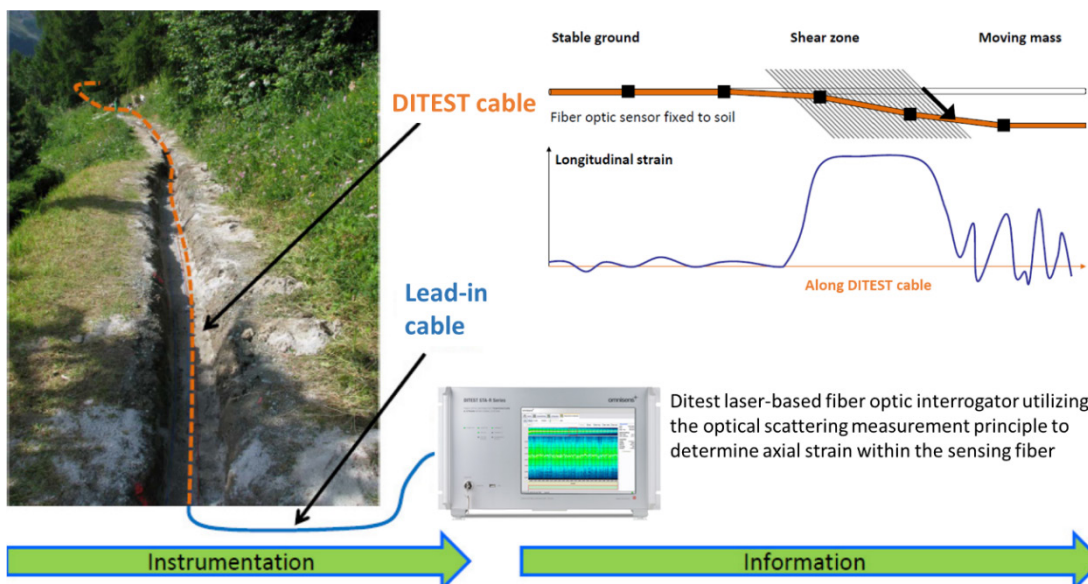
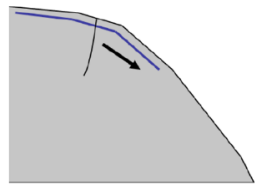
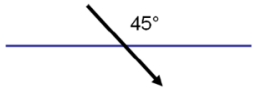
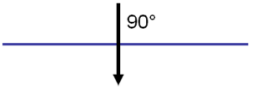


Figure 4.24 DITEST cable used for monitoring ground deformations in this case creep across a slope (Marmota 2012)

Sensitivity of fiber optic cables is quite high for detecting strain and seabed deformation provided that the cable is well connected to the seabed (embedded), see Table 4.1.

Table 4.1 Resolution, accuracy and range for deformations relative the strain cable (Marmota 2012)

Example	Sensor crossing a crack opening due to a creeping landslide	Sensor crossing a creeping landslide boundary at 45°	Sensor crossing a creeping landslide boundary at approx. 90°
			
System resolution	0.02 mm/m of soil movement	0.03 mm/m of soil movement	0.2 mm/m of soil movement
System accuracy	0.1 mm/m of soil movement	0.2 mm/m of soil movement	2 mm/m of soil movement 0.2 mm/m with enhanced configuration
Sensor range	+ 20 mm/m - 5 mm/m	± 30 mm of soil movement	± 200 mm of soil movement

The resolution in the measurements also depends on the length of the fiber optic strain cable and the spatial resolution of the measuring points. As can be seen in the diagram below (Figure 4.25) a resolution of some μ strain can be expected for the test cable with measurement at each meter. The amount of readings (averaging time) will improve the resolution, 5-10 minutes of scanning time must be collected for each complete set of readings

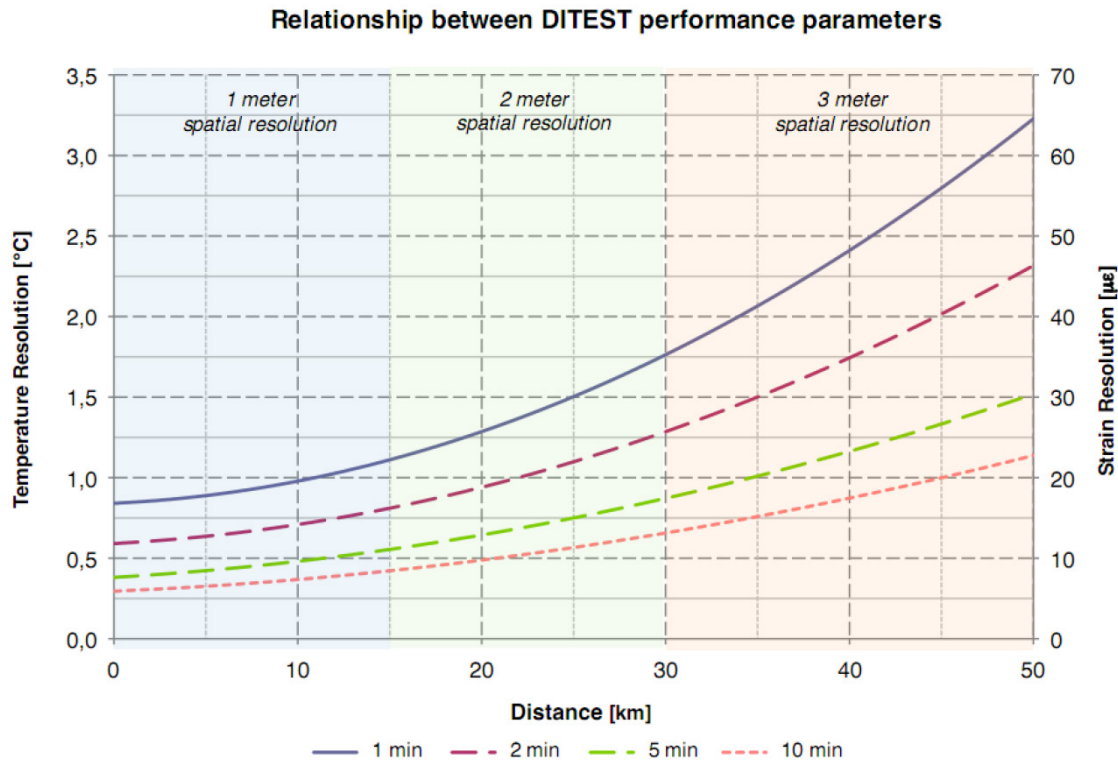


Figure 4.25 Resolution of temperature and strain readings depend on cable length, spatial resolution and time for reading (Diserens 2017)

No preparation of the optical fiber is required for distributed sensing and a network of fibre optic telecom and data cables can be used for detection of seismic events and seafloor deformations in the future (though this will not offer the resolution of specialist fibers). For standalone operation, the present challenge is that most of the fiber optic laser interrogators in the market are power intensive and best suited for operation at the surface. However, this is an emerging technology sector that is evolving quickly and solutions suitable for subsea operation are expected within a short time. Cable arrays for distributed sensing can possibly be hooked up and operated via control umbilical cord to CO₂ injection wells. Fiber optic cables embedded in the seabed with combined Brillouin (DITEST) and Rayleigh (DAS/DVS) monitoring can be used to monitor permanent seabed deformations as well as micro seismic activity.

4.4 Systems proposed for testing and evaluation at seafloor in SENSE

As part of the SENSE project, nearshore tests are planned in the Bay of Mecklenburg with ideal conditions (sand under clay) for shallow injection tests, see Figure 4.26. Some of the described monitoring solutions will be deployed during this test. The advantage of this location is a lower cost installation from which data can be downloaded directly by means of a lead-in cable to shore. The nearshore test site will provide data and knowledge on functionality, background noise and drift in the data readings. Some equipment (sensors) will be identical to instruments used in more remote locations in deep water. Sensor enclosures used during the SENSE tests may be rated for shallow waters, but more robust casings are available. For benchmark design, information about the sediment conditions are required and the bathymetry at the site must be well known.

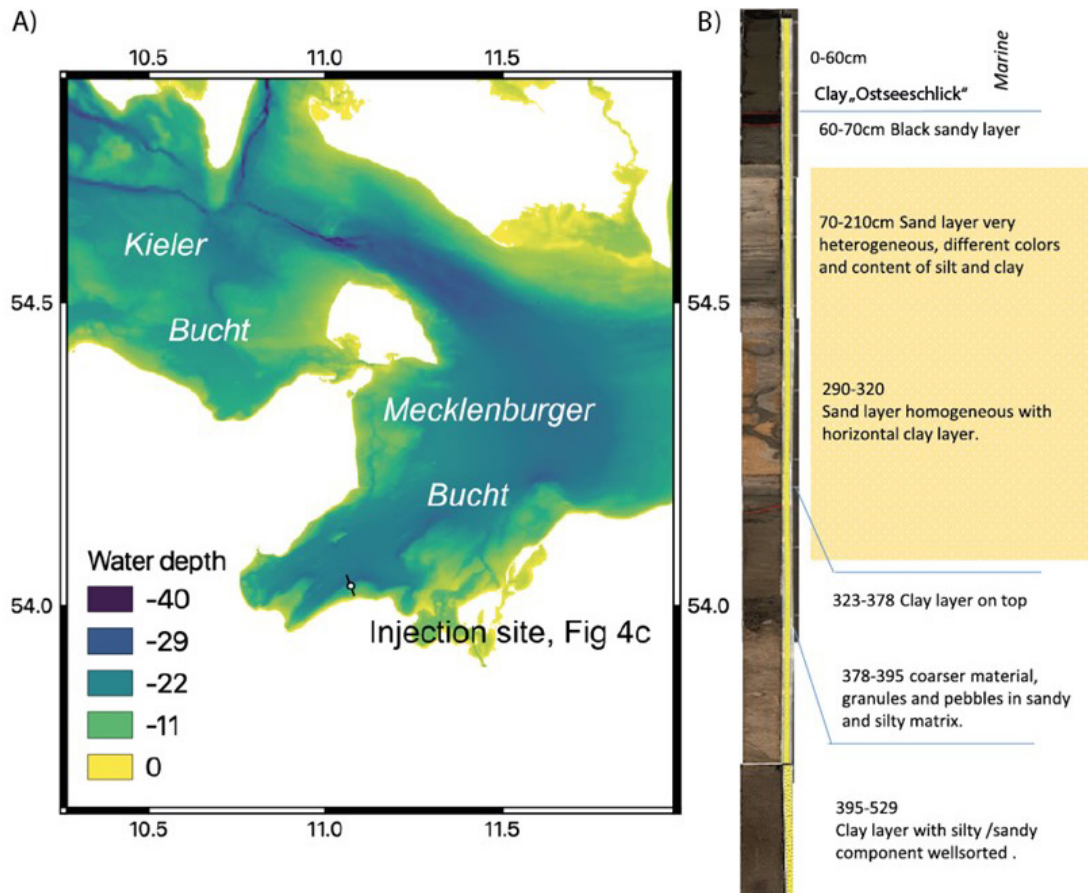


Figure 4.26 Proposed location for injection tests and preliminary soil conditions

4.4.1 Combined tilt and pressure recording unit (Geomar)

We plan to combine accelerators, tilt and pressure recordings in one compact unit that can fit on a benchmark and easily be recovered after a long recording period. The intention and first choice is to use the SOS module from Paroscientific. The inbuilt data logger has a low power consumption and sufficient resolution to match the precision tilt and pressure sensors.

The pressure sensors will have a range of up to 2000 m water depth and it is recommended to include the self-calibrating feature to enable reliable data collection during long term deployment. The logger will be programmed for the desired logging schedule including a trigger function for more rapid sampling, triggered by, for example, a tilt event. The battery and recording capacity is at least two years. Data can be downloaded by cable (shore tests) and may be transmitted by acoustic or other types of subsea modems (not included for the testing phase). The standard enclosure rating is 2000 or 3000 m (titanium enclosures) but for nearshore tests cheaper POM enclosures may be used. The pore pressure and tilt unit can be deployed using a lander developed by GEOMAR (Figure 4.27).

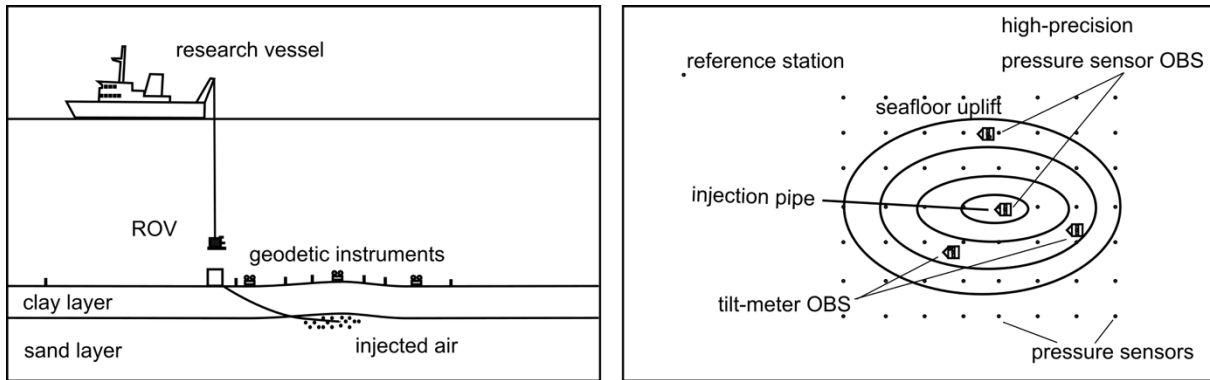


Figure 4.27 Schematic sketch of the experiment and survey layout

4.5 Fibre optic seabed cable for distributed sensing (NGI)

As a separate installation, it is planned that a fibre optic strain cable (DITEST) will be installed across the expected uplift area, see Figure 4.28. The cable will be routed across the seabed area expected to be affected by the injection tests for deformation monitoring. The fibre must be secured to the seabed to prevent motion by water current (embedded or buried by sand/gravel). A lead-in cable section will transfer the fibre optic signals to shore and a land based laser interrogator, see figure Figure 4.28. The strain cable end will be equipped with a termination anchor and the start of the lead-in will be secured by a clump-weight. If an internet connection is available, it may be possible to remotely operate the system by a remote desktop or similar arrangement.

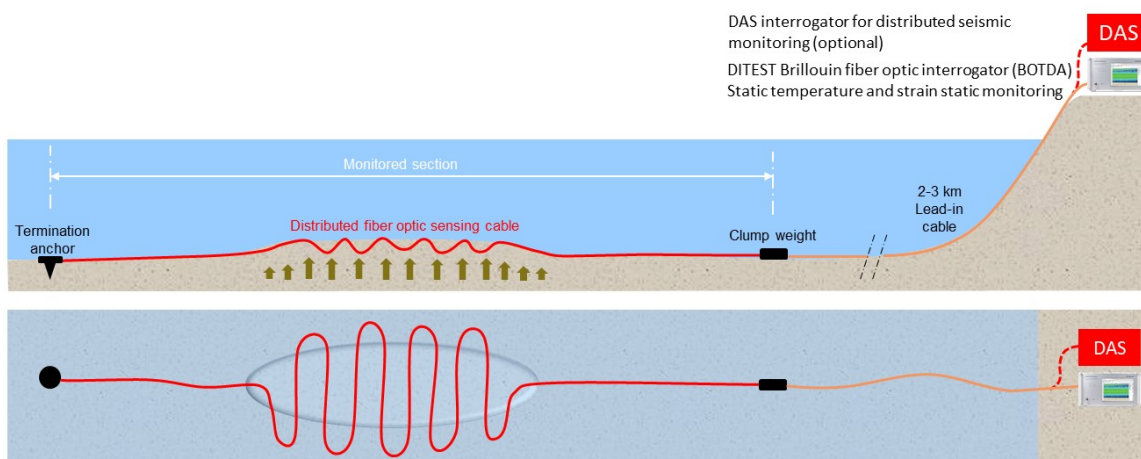


Figure 4.28 A schematic presentation of fibre optic deployment in a shallow water site close to the shore.

The BOTDR laser fibre optic interrogator (see Figure 22) must be placed indoor with a power supply, in addition a PC with Diview software is required. With internet access this PC may be controlled remotely.

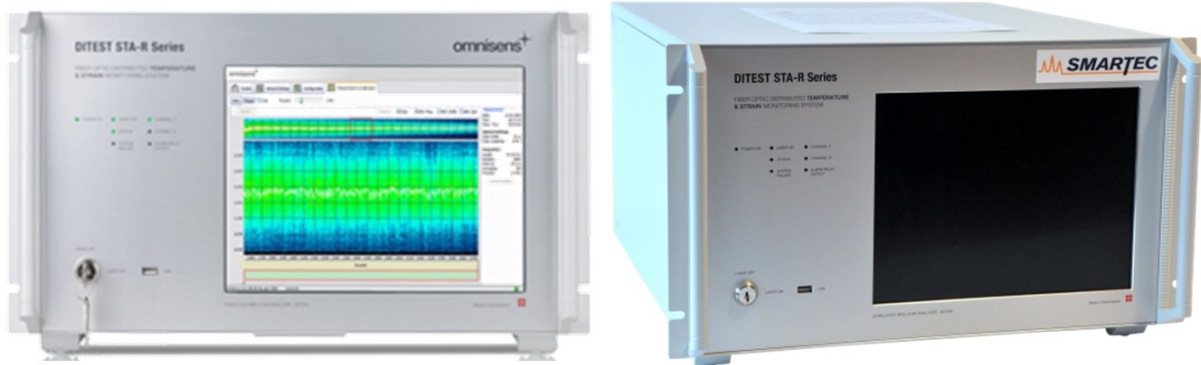


Figure 4.29 DITEST BOTDA mode laser interrogator for distributed temperature and strain measurements (Brillouin static measurements)

We are presently considering the possibility of including a DAS interrogator from Alcatel Submarine Networks (Huchet and Brenne 2018) in the land based DAQ system such that the fibre optic strain cable also can be used for distributed seismic recordings across the uplift test area

Acknowledgement

SENSE (Assuring integrity of CO₂ storage sites through ground surface monitoring) project No. 299664, has been subsidized through ACT (EC Project no. 691712) by Gassnova, Norway, United Kingdom Department for Business, Energy and Industrial Strategy, Forschungszentrum Jülich GMBH, Projektträger Jülich, Germany, The French Agency for the Environment and Energy Management, The United States Department of Energy, State Research Agency, Spain, with additional support from Equinor and Quad Geometrics.

References

- ACT Call, 2018. Accelerating CCS Technologies. New ACT Call, June 2018. <http://www.act-ccs.eu/calls/>
- Agisco, 2019. Consulting the website: <https://www.agisco.it/en/prodotti/strumenti-di-misura-sensori/>
- Bamler, R. and Hartl, P., 1998. "Synthetic aperture radar interferometry", *Inverse Problems*, vol. 14, pp. R1–54
- Bateson, L., Cigna, F., Boon, D., Sowter, A., 2015. The application of the ISBAS InSAR method to the South Wales Coalfield. *International Journal of Applied Earth Observation and Geoinformation*, 34, 249-257. <https://doi.org/10.1016/j.jag.2014.08.018>
- Berardino, P., Fornaro, G., Lanari, R., Sansosti E., 2002. "A new algorithm for surface deformation monitoring based on small baseline differential SAR interferograms", *IEEE Trans. Geosciences and Remote Sensing*, 40, 2375– 2383
- Bjørnarå, T. I., Nordbotten, J. M., Park, J., 2016. Vertically integrated models for coupled two-phase flow and geomechanics in porous media. *Water Resources Research*, 52(2):1398–1417
- Bjørnarå, T.I., Bohloli, B. and Park, J., 2018. Field-data analysis and hydromechanical modeling of CO₂ storage at In Salah, Algeria. *Int. J. Greenh. Gas Contr.* 79, 61–72
- Bohloli, B., Ringrose, P., Grande, L., Nazarian, B., 2017. Determination of the fracture pressure from CO₂ injection time-series datasets. *Int. J. Greenhouse Gas Control* 61, 85-93
- Bohloli, B., Bjørnarå, T.I., Park, J., Rucci, A., 2018. Can surface uplift be used as a tool for monitoring reservoir performance? A case study from In Salah, Algeria. *Int. J. Greenhouse Gas Control* 76, 200-207
- Boni, R., Bosino, A., Meisina, C., Novellino, A., Bateson, L., McCormack, H., 2018. A methodology to detect and characterize uplift phenomena in urban areas using Sentinel-1 data. *Remote Sensing*, 10 (4), 607. <https://doi.org/10.3390/rs10040607>
- Bui, M., Adjiman, C.S., Bardow, A., Anthony, E.J., Boston, A., Brown, S., Fennell, P.S., Fuss, S., Galindo, A., Hackett, L.A., Hallett, J.P., Herzog, H.J., Jackson, G., Kemper, J., Krevor, S., Maitland, G.C., Matuszewski, M., Metcalfe, I.S., Petit, C., Puxty, G., Reimer, J., Reiner, D.M., Rubin, E.S., Scott, S.A., Shah, N., Smit, B., Trusler, J.P.M., Webley, P., Wilcox, J., Mac, Dowell, N., 2018. Carbon capture and storage (CCS): the way forward. (Review Article) *Energy Environ. Sci.*, 2018, 11, 1062-1176. DOI: 10.1039/C7EE02342A
- Bürgmann, R., Chadwell, D., 2014. Seafloor geodesy. *Annual Review of Earth and Planetary Sciences*, 42, 509-534
- Bürgmann, R., Rosen, P. A., Eric, J., 2000. "Fielding Synthetic Aperture Radar Interferometry To Measure Earth's Surface Topography And Its Deformation", *Annu. Rev. Earth Planet. Sci.*, vol. 28, pp 169–209

Cavanagh, A., Ringrose, P.S., 2011. Simulation of CO₂ distribution at the In Salah storage site using high-resolution field-scale models. *Energy Procedia* 4, 3730–3737

CCS and CCU Implementation Plan, 2017. SET Plan ACTION NO 9 –Implementation Plan- 21 09 2017. SET-PLAN TWG9 CCS and CCU Implementation Plan, https://setis.ec.europa.eu/system/files/set_plan_ccus_implementation_plan.pdf

Cespa, S., Del Conte, S., Giannico, C., Ferretti, A., Iannicella, I., 2016. 15 years of satellite interferometry: state of the art and new trends. *Gallerie e grandi opera sotteranee*, no. 118/June 2016 (in Italian)

Chadwick, R.A., Eiken, O., 2013. Offshore CO₂ storage: Sleipner natural gas field beneath the North Sea. *Geological Storage of Carbon Dioxide (CO₂): Geoscience, Technologies, Environmental Aspects and Legal Frameworks*, Woodhead Publishing, pages 227–250

Chadwick, A., Arts, R., Bernstone, C., May, F., Thibeau, S., Zweigel, P., 2008. Best practice for the storage of CO₂ in saline aquifers-observations and guidelines from the SACS and CO₂STORE projects, Report 289 Pages. <http://www.sciencedirect.com/science/article/pii/S0034425714002454>

Chan, A.W., 2004. Production-induced reservoir compaction, permeability loss and land surface subsidence. PhD Dissertation. Dep. Geophysics, Stanford University, USA. Darling, T., 2006. *Krechba overburden review*. BP Report. 50 p

Colóna, C., Webb, A.A.G., Lasserrec, C., Doinc, M.-P., Renard, F., Lohman, R., Li, L., Baudoin, P. F., 2016. The variety of subaerial active salt deformations in the Kuqa fold-thrust belt (China) constrained by InSAR. *Earth and Planetary Science Letters* 450 (2016) 83–95

Costantini, M., Rosen, P. A., 1999. A Generalized Phase Unwrapping Approach for Sparse Data. *IEEE International Geoscience & Remote Sensing Symposium* 1: 267–269, Hamburg, Germany.

Deflandre, J.P., Estublier, A., Baroni, A., Daniel, J.M., Adjémian, F., 2011. In Salah CO₂ injection modeling: a preliminary approach to predict short term reservoir behavior. *Energy Procedia* 4, 3574–3581

Diserens, A., 2017. Increasing Dam Safety and Integrity by using Distributed Fibre Optic Sensing (DFOS). Third national Dam Safety Conference, 18-19 Feb. 2017 Roorkee, India

Dunn, S., Hatchell, P., van den Beukel, A., de Vries, R., Frafjord, T., 2016. A long-term seafloor deformation monitoring campaign at Ormen Lange gas field. *First Break*, 34(10), 55-64

Eiken, O., Stenvold, T., Zumberge, M., Alnes, H., Sasagawa, G., 2008. Gravimetric monitoring of gas production from the Troll field. *GEOPHYSICS VOL. 73, NO. 6, November-December 2008*; P. WA149–WA154, 10.1190/1.2978166

Eide, L.I., 2012. GEOSS, Report on Task SB-05 - Impact Assessment of Human Activities Component C3 – Operational Carbon Capture and Sequestration (CCS) Monitoring System, a feasibility study. Final report GEOSS SB-05 C3. 52 p

Eiken, O., Ringrose, P., Hermanrud, C., Nazarian, B., Torp, T.A., Høier, L., 2011. Lessons Learned from 14 years of CCS Operations: Sleipner, In Salah and Snøhvit. *Energy Procedia* 4, 5541–5548

Ferretti, A., Prati, C., Rocca, F., 2000. Nonlinear subsidence rate estimation using permanent scatterers in differential SAR interferometry. *IEEE Transactions on Geoscience and Remote Sensing*. Volume: 38, Issue: 5, Sep 2000

Ferretti, A., Prati, C., and Rocca, F., 2001. Permanent scatterers in SAR interferometry, *IEEE Transactions on Geoscience and Remote Sensing*, 39, pp 8-20

Ferretti, A., Fumagalli, A., Novali, F., Prati, C., Rocca, F. and Rucci, A., 2011. A new algorithm for processing interferometric data-stacks: SqueeSAR. *IEEE Transactions on Geoscience and Remote Sensing*, 49(9), pp.3460-3470. DOI: 10.1109/TGRS.2011.2124465

Ferretti, A., Novali, F., Rucci, A., 2012. Monitoring ground movement over In Salah (Algeria) using SqueeSARTM. In: Report to JIP. November 2011–January 2012, XBand Data. Ref.: JO11-0049-REP3.0

Freiburg, J.T., Morse, D.G., Leetaru, H.E., Hoss, R.P., Yan Q., 2014. A depositional and diagenetic characterization of the Mt. Simon Sandstone at the Illinois Basin - Decatur Project carbon capture and storage site, Decatur, Illinois, USA: Illinois State Geological Survey, Circular 583, 59 p

Furre, A.K., Eiken, O., Alnesa, H., Nesland Veatne, J., Kiær, A.F., 2017. 20 years of monitoring CO₂-injection at Sleipner. *Energy Procedia* 114, 3916 – 3926

Gee, D.; Bateson, L.; Sowter, A.; Grebby, S.; Novellino, A.; Cigna, F.; Marsh, S.; Banton, C.; Wyatt, L., 2017. Ground Motion in Areas of Abandoned Mining: Application of the Intermittent SBAS (ISBAS) to the Northumberland and Durham Coalfield, UK. *Geosciences* 7, 85. <https://doi.org/10.3390/geosciences7030085>

Gens, R., Vangenderen, J. L., 1996. SAR interferometry – Issues, techniques, applications, *Intl. J. Remote Sensing*, vol. 17, no. 10, pp. 1803–1835

Goertz-Allmann, B.P., Kühn, D., Oye, V., Bohlooli, B., Aker, E., 2014. Combining micro-seismic and geomechanical observations to interpret storage integrity at the In Salah CCS site. *Geophys J. Int.* 198 (1), 447-461

Goldfeld, Y., Klar, A., 2013. Damage Identification in Reinforced Concrete Beams Using Spatially Distributed Strain Measurements. *Journal of Structural Engineering / Volume 139 Issue 12 - December 2013*

Hannis, S., Chadwick, A., Connelly, D., Blackford, J., Leighton, T., Jones, D., White, J., White, P., Wright, I., Widdicomb, S., Craig, J., Dixon, T., 2017. Review of offshore CO₂ storage monitoring: operational and research experiences of meeting regulatory and technical requirements. *Energy Procedia* 114 (2017) 5967 – 5980

Hettema, M., Papamichos, E., Scutjens, P., 2002. Subsidence delay: field observations and analysis. *Oil and Gas Science and Technology. Revue d'IFP Energies Nouvelles*, Institut Francais du Petrole, 57(5), pp. 443-458. 10.2516/ogst:2002029, hal-02043963

Hicke, K., 2019. Distributed fibre optic sensing for monitoring and testing of industrial and civil infrastructures. InnoTesting Conference 2018, Wildau, Germany, 23.02.2018

Huchet, G., Brenne, J.K., 2018. FIBER SENSING IS EVERYWHERE: Distributed Acoustic Sensing For Submarine Telecommunication Systems. SUBMARINE TELECOMS FORUM issue 102/September 2018

Iding, M., Ringrose, P., 2010. Evaluating the impact of fractures on the performance of the In Salah CO₂ storage site. *Int. J. Greenh. Gas Control* 4 (2), 242–248. Mathieson, A., Wright, I., Roberts, D.M., Ringrose, P.S., 2009. Satellite imaging to monitor CO₂ movement at Krechba, Algeria. *Energy Procedia* 1, 2201–2209

IEAGHG, 2011. Feasibility of monitoring techniques for substances mobilised by CO₂ storage in geological formations. Report 2011/08, December 2011. Accessed 02-12-2019 at: https://ieaghg.org/docs/General_Docs/Reports/2011-08.pdf

IEAGHG, 2017. 12th IEAGHG monitoring network meeting. 13th-15th June, Michigan, USA

Jenkins, C., Chadwick, A., Hovorka S.D., 2015. The state of the art in monitoring and verification—Ten years on. *International Journal of Greenhouse Gas Control* 40 (2015) 312–349

Jordan, C. J., Bateson, L., Novellino, A., 2019. Environmental baseline monitoring for shale-gas development: Insights for monitoring ground motion using InSAR analysis. *Science of the Total Environment*, 696, 134075. <https://doi.org/10.1016/j.scitotenv.2019.134075>

Jordan, H., Cigna, F., Bateson, L., 2017. Identifying natural and anthropogenically-induced geohazards from satellite ground motion and geospatial data: Stoke-on-Trent, UK. *International Journal of Applied Earth Observation and Geoinformation*, 63. 90-103. <https://doi.org/10.1016/j.jag.2017.07.003>

Karstens, J., Berndt, C., 2015. Seismic chimneys in the Southern Viking Graben –Implications for palaeo fluid migration and overpressure evolution. *Earth & Planetary Science Letters* 2015;412: 88-100

Kim, J.W., Lu, Z., 2018. Association between localized geohazards in West Texas and human activities, recognized by Sentinel-1A/B satellite radar imagery. *Scientific Reports* 8(1), DOI: 10.1038/s41598-018-23143-6

Lang, D., Kopp, H., Royer, J.Y., Henry, P., Çakir, Z., Petersen, F., Sakic, P., Ballu, V., Bialas, J., Özeren, M.S., Ergintav, S., Géli, L., 2019. Interseismic strain build-up on the submarine North Anatolian Fault offshore Istanbul. *Nature Communications* volume 10, Article number: 3006

Litynski, J., Vikara, D., Webster, M., Srivastava, R., 2013. U.S. Department of Energy Efforts to Advance Remote Sensing Technologies for Monitoring Geologic Storage Operations. *Energy Procedia* 37 (2013) 4114 – 4127, DOI: 10.1016/j.egypro.2013.06.313

Locke, R., 2017. The Illinois Basin-Decatur Project: surface and near surface monitoring protocols. IEAGHG Monitoring Network Meeting, June 15, 2017, Traverse City, Michigan Presentation file available (20-12-2019): https://ieaghg.org/docs/11mon/Session8_Talk5_2017%2006%2015_IEAGHG%20Mon%20Net_Locke.pdf

Madsen, S. N., and Zebker, H. A., 1999. Synthetic aperture radar interferometry: Principles and applications,” *Manual of Remote Sensing*. Boston, MA: Artech House, vol. 3, ch. 6

Marmota 2012, GeoScan Documentation Marmota Engineering AG, consult the website <https://www.marmota.com/index.php>

Massonnet, D. Feigl, K. L., 1998. Radar interferometry and its application to changes in the earth's surface", Rev. Geophys., vol. 36, no. 4, pp. 441–500

Mathieson, A., Midgely, J., Wright, I., Saoula, N., Ringrose, P., 2011. In Salah CO2 Storage JIP: CO2 sequestration monitoring and verification technologies applied at Krechba, Algeria. Energy Procedia 4 (2011) 3596–3603

Mathieson, A., Midgley, J., Dodds, K., Wright, I., Ringrose, P., Saoula, N., 2010a. CO2 sequestration monitoring and verification technologies applied at Krechba, Algeria. Lead. Edge 29(2), 216–222

Mathieson, A., Midgley, J., Wright, I., Saoula, N., Ringrose, P., 2010b. In Salah CO2 Storage JIP: CO2 sequestration monitoring and verification technologies applied at Krechba, Algeria. Energy Procedia 4, 3596–3603

Morris, J.P., Hao, Y., Foxall, W., McNab, W. 2011. A study of injection-induced mechanical deformation at the In Salah CO2 storage project. International Journal of Greenhouse Gas Control 5, 270–280

Mission innovation CCUS, 2017. Mission innovation, accelerating the clean energy revolution, Carbon Capture Innovation Challenge, Report of the Carbon Capture, Utilization and Storage Experts' Workshop September 26–28, 2017 Houston, Texas. Available from https://www.energy.gov/sites/prod/files/2018/05/f51/Accelerating%20Breakthrough%20Innovation%20in%20Carbon%20Capture%2C%20Utilization%2C%20and%20Storage%20_0.pdf

McCormack, H., Bateson, L., Banton, C., Holley, R., Lawrence, D., Cigna, F., Watson, I., and Burren, R. 2013. Surface deformation in areas of abandoned mining: a case study of InSAR applied in the Northumberland region of the UK. Geophysical Research Abstracts Vol. 15, EGU2013-11551-1, 2013 EGU General Assembly 2013

Nordbotten J.M., Celia M.A., Bachu S., 2005. Injection and storage of CO2 in Deep saline aquifers: analytical solution for CO2 plume evolution during injection. Transp. Porous Media 58(3), 339–360

Nooner, S.L., Eiken, O., Hermanrud, C., Sasagawa, G.S., Stenvold, T., Zumberge, M.A. 2007. Constraints on the in situ density of CO2 within the Utsira formation from time-lapse seafloor gravity measurements. International Journal of greenhouse gas control Vol. 1, pp 198 – 214

Octio, 2019. Gravitude gwatch: 4D gravity at the seafloor. <http://www.octio.com/4d-gravity-at-the-seafloor/>

Octio Gravitude, 2019. Octio gravitude obtains unprecedented data quality at the snøhvit, albatross and askeladd fields. Accessed 03-12-2019 at: <https://www.octio.com/octio-gravitude-obtains-unprecedented-data-quality-at-the-snohvit-albatross-and-askeladd-fields/>

Onuma, T., Ohkawa, S., 2009. Detection of surface deformation related with CO2 injection by DInSAR at In Salah, Algeria. Energy Procedia 1, 2177–2184

Oye, V., Zhao, P., Kühn, D., Iranpour, K., Aker, E., Bohloli, B., 2012. Monitoring of the Krechba, In Salah, CO₂ storage using microseismic data analysis. In: Third EAGE CO₂ Geological Storage Workshop. 26–27 March 2012, Edinburgh, UK

Paros, J.M., Kobayashi, T., 2018. Calibration Methods to Eliminate Quartz Sensor Drift. Technical Note, Doc. No. G8097 Rev. K. Published on website:
http://paroscientific.com/pdf/G8097_Calibration_Methods_to_Eliminate_Sensor_Drift.pdf

Petrat, L., Riedmann, M., Anderssohn, J. 2011. CO₂ Storage– Monitoring of Related Surface Movements from Space - Potential for Central European Land Cover Conditions? 73rd EAGE Conference and Exhibition incorporating SPE EUROPEC 2011

Petersen, F., Kopp, H., Lange, D., Hannemann, K., Urlaub, M., 2019. Measuring tectonic seafloor deformation and strain-build up with acoustic direct-path ranging. *Journal of Geodynamics*

Polster, A., Fabian, M., Villinger, H., 2009. Effective resolution and drift of Paroscientific pressure sensors derived from long-term seafloor measurements. *Geochemistry, Geophysics, Geosystems*, 10(8)

Quad Geometrics, 2019. Consulting the website: <https://quadgeo.com/>

Rinaldi, A.P., Rutqvist, J., 2013. Modeling of deep fracture zone opening and transient ground surface uplift at KB-502 CO₂ injection well, In Salah, Algeria. *Int. J. Greenh. Gas Control* 12, 155–167

Ringrose, P., Atbi, M., Mason, D., Espinassous, M., Myhrer, O., Iding, M., Mathieson, A., Wright, I., 2009. Plume development around well KB-502 at the In Salah CO₂ storage site. *First Break*. 27, 49–53

Ringrose, P.S., Mathieson, A., Wright, I., Selama, F., Hansen, O., Bissell, R., Saoula, N., Midgley, J., 2013. The In Salah CO₂ Storage Project: Lessons Learned and Knowledge Transfer. *Energy Procedia* 37 (2013) 6226-6236

Ringrose, P., Roberts, D.M., Gibson-Poole, C.M., Bond, C., Wightman, R., Taylor, M., Raikes S., Iding, M., Ostmo, S., 2010. Characterisation of the Krechba CO₂ storage site: critical elements controlling injection performance. *Energy Procedia* 4, 4672–4679

Rocca, F., Prati, C., Ferretti, A., 1997. An Overview of SAR Interferometry, Proc. 3rd ERS Symposium, Florence, <http://florence97.ers-symposium.org>, 1997

Rock, L., O'Brien, S., 2016. Carbon Capture and Storage: the QUEST Project. AAPG 2016 Annual Convention and Exhibition, Calgary, Alberta, Canada, June 19-22, 2016. Accessed 02-12-2019: http://www.searchanddiscovery.com/documents/2017/80577rock/ndx_rock.pdf

Rosen, P. A., Hensley, S. and Joughin, I., Li, F., Madsen, S., Rodriguez, E., and Goldstein, R., 2000. Synthetic Aperture Radar Interferometry, Proc. IEEE, pp. 333–379

Rutqvist, J., Vasco, D.W., Majer, E., Liu, H.H., Kappler, K., Pan, L., 2010a. In: Coupled Thermal, Hydraulic and Geomechanical Numerical Modeling for Interpretation of Ground Surface Deformations and Potential of Injection-Induced Micro-Earthquakes, Ninth Annual Conference on Carbon Capture & Sequestration. Pittsburgh, USA. April 2010

Rutqvist, J., Liu, H.H., Vasco, D.W., Pan, L., Kappler, K., Majer, E., 2010b. Coupled non-isothermal, multiphase fluid flow, and geomechanical modeling of ground Surface deformations and potential for induced micro-seismicity at the In Salah CO₂ storage operation. Proc. GHGT-10, Amsterdam, 19-23 September, 2010

Rucci, A., Vasco, D. W., Novali, F., 2013. Monitoring the geological storage of carbon dioxide using multi-component SAR interferometry, *Geophysical Journal International*, 193, 197-208, doi: 10.1093/gji/ggs112

Rutqvist, J., Vasco, D.W., Myer, L., 2009. Coupled reservoir-geomechanical analysis of CO₂ injection at In Salah, Algeria. *Energy Procedia* 1, 1847–1854

Shi, J.-Q., Sinayuc, C., Durucan, S., Korre, A., 2012. Assessment of carbón dioxide plume behaviour within the storage reservoir and the lower caprock around the KB-502 injection well at In Salah. *Int. J. Greenh. Gas Control.* 7, 115–126

Shi, J.-Q., Smith, J., Durucan, S., Korre, A., 2013. A Coupled Reservoir Simulation-Geomechanical Modelling Study of the CO₂ Injection-Induced Ground Surface Uplift Observed at Krechba, In Salah, GHGT-11 Vol: 37, pp. 3719–3726 ISSN:1876-6102

Shi, J.Q., Sevket, D., Korre, A., Ringrose, P., Mathieson, A., 2019. History matching and pressure analysis with stress dependent permeability using the In Salah CO₂ storage case study. *Int. J. Greenhouse Gas Tech.* 91, 102844

Spieß, F.N., 1995. Suboceanic geodetic measurements. *IEEE transactions on geoscience and remote sensing* (4), 502-510

Teatini, P., Gambolati, G., Ferronato, M., Settari, A., Walters, D., 2011. Land uplift due to subsurface fluid inection. *J. Geodyn.* 51, 1–16

TRE, 2019. TRE ALTAMIRA, Historical analysis. Available on <https://site.tre-altamira.com/insar-solutions/insar-historical-analysis/>

Urlaub, M., Petersen, F., Gross, F., Bonforte, A., Puglisi, G., Guglielmino, F., Lange D., Kopp, H. 2018. Gravitational collapse of Mount Etna’s southeastern flank. *Science advances*, 4(10), eaat9700

Urlaub, M., Villinger, H., 2019. Combining in situ monitoring using seabed instruments and numerical modelling to assess the transient stability of underwater slopes. Geological Society, London, Special Publications, 477(1), 511-521, eaat9700

Urlaub, M., Villinger, H. (2019). Combining in situ monitoring using seabed instruments and numerical modelling to assess the transient stability of underwater slopes. Geological Society, London, Special Publications, 477(1), 511-521

van den Beukel, A., Zainuddin, M.J., Riddell, P., Noraberg, K.T., Hodgson, N., Naujoks, M., Glegola, M., Bomers, M., Liu, S., 2014. Integrated Reservoir Monitoring of the Ormen Lange field: Time lapse seismic, Time lapse gravity and seafloor deformation monitoring. Biennial Geophysical Seminar “Broadband seismic – the next revolution in geophysical exploration” Kristiansand, Norway, 17-19 March 2014

Vasco, D.W., Ferretti, A., Novali, F. 2008a. Reservoir monitoring and characterization using satellite geodetic data: Interferometric synthetic radar observations from the Krechba field Algeria. *Geophysics*, 73 (6) (2008), pp. WA113-WA122

Vasco, D.W., Ferretti, A., Novali, F., 2008b. Estimating permeability from quasi-static deformation: temporal variations and arrival-time inversion. *Geophysics* 73 (6), O37–O52

Vasco, D.W., Rucci, A., Ferretti, A., Novali, F., Bissell, R.C., Ringrose, P.S., Mathieson, A.S., Wright, I.W., 2010. Satellite-based measurements of surface deformation reveal fluid flow associated with the geological storage of carbon dioxide. *Geophys. Res. Lett.* 37, L03303

Vatshelle, M., Glegola, M., Lien, M., Noble, T., Ruiz, H., 2107. Monitoring the Ormen Lange field with 4D gravity and seafloor subsidence. 79th EAGE Conference & Exhibition, Paris, France. DOI: 10.3997/2214-4609.201700484

Verdon, J.P., Kendall, J., Stork, A.L., Andy, R., Chadwick, D., White, J., Bissell, R.C., 2013. Comparison of geomechanical deformation induced by megatonne-scale CO₂ storage at Sleipner, Weyburn, and In Salah. *PNAS* July 23, 2013. 110 (30) E2762-2771; <https://doi.org/10.1073/pnas.1302156110>

White, J.A., Chiaramonte, L., Ezzedine, S., Foxall, W., Hao, Y., Ramirez, A. and McNab, W., 2014. Geomechanical behavior of the reservoir and caprock system at the In Salah CO₂ storage project. *Proceedings of the National Academy of Sciences*, p.201316465

White, J.A., Chiaramonte, L., Ezzedine, S., Foxall, W., Hao, Y., Ramirez, A., McNab, W., 2014. Geomechanical behavior of the reservoir and caprock system at the In Salah CO₂ storage project *PNAS* | June 17, 2014, vol. 111, no. 24, 8747–8752

Worth, K., D. White, D., Chalaturnyk, R., Sorensen, J., Hawkes, C., Rostron, B., Johnson, J., Young, A., 2014. Aquistore Project Measurement, Monitoring, and Verification: From Concept to CO₂ Injection. *Energy Procedia* 63, 3202 – 3208

Wöfl, A.C., Snaith, H., Amirebrahimi, S., Devey, C.W., Dorschel, B., Ferrini, V., Huvenne, V.A.I., Jakobsson, M., Jencks, J., Johnston, G., Lamarche, G., Mayer, L., Millar, D., Pedersen, T.H., Picard, K., Reitz, A., Schmitt, T., Visbeck, M., Weatherall, P., Wigley, R., 2019. Seafloor Mapping – The Challenge of a Truly Global Ocean Bathymetry. *Front. Mar. Sci.* 6:283 Available from: https://www.researchgate.net/publication/333639078_Seafloor_Mapping_-_The_Challenge_of_a_Truly_Global_Ocean_Bathymetry [accessed Dec 21 2019]

Xue, Z., Shi, J.Q., Yamauchi Y., Durucan S., 2018. Fiber Optic Sensing for Geomechanical Monitoring: (1)-Distributed Strain Measurements of Two Sandstones under Hydrostatic Confining and Pore Pressure Conditions. *Appl. Sci.* 2018, 8, 2103; doi:10.3390/app8112103

Yang, C., Lu, Z., Zhang, Q., Liu, R., Ji, L., Zhao, C., 2019. Ground deformation and fissure activity in Datong basin, China 2007–2010 revealed by multi-track InSAR Geomatics, *Natural Hazards and Risk* 10(1):465-482

Zhang, Y., Meng, X., Jordan, C., Novellino, A., Dijkstra, T. and Chen, G., 2018. Investigating slow-moving landslides in the Zhouqu region of China using InSAR time series. *Landslides*, 15(7), pp.1299-1315. doi:10.1007/s10346-018-0954-8

Zheng, W., Kim, J.W., Syed Tabrez, A., Lu, Z., 2019. Wastewater leakage in West Texas revealed by satellite radar imagery and numerical modelling. December 2019, *Scientific Reports* 9(1), DOI: 10.1038/s41598-019-51138-4

Zweigel, P., Arts, R., Lothe, A.E., Lindeberg, E., 2004. Reservoir geology of the utsira formation at the first industrial-scale underground CO₂ storage site (Sleipnerarea, North Sea). In: Baines S., Gale J., Worden R. (Eds.), *Geological Storage of Carbon Dioxide for Emissions Reduction*. Geological Society, London, pp. 165–1802004

Appendix A – InSAR Terminology and Working Concept

A1. InSAR Terminology

RADAR is an abbreviation for "RADio Detection And Ranging". Radar systems are active systems, consisting of both a transmitter and a receiver. By recording the backscattered return signal from the transmitted electrical pulse, distance, direction and the scattering properties of the object is measured. Radar waves are in the microwave region of the electromagnetic spectrum and are mostly free from atmospheric disturbances such as clouds, rain, fog, etc. Since these systems are active, they can gather information at any time during day and night. The components of the radar waves are the phase and the intensity, both containing information of relevance to the application of SAR data.

SAR, Synthetic Aperture Radar, is a more advanced application of radar imagery, where a larger antenna is synthesized by using the so-called Doppler principle. Larger antennas enable a higher resolution and better ground information with sub-meter accuracy. Developing this principle further, the phase information from the complex images acquired by the SAR sensor, is used to extract topographic information from the ground surface.

This is InSAR, i.e. Interferometric SAR, where processing the same portion of ground surface from different view angles results in an interferogram, also called a phase difference image. From such phase difference images, heights can be extracted in order to produce high accuracy digital elevation models (DEMs). An interferogram may also contain the phase information due to displacement of the ground surface. The extraction of such displacements needs some extra efforts in order to separate them from the topographic phases.

Differential SAR Interferometry (DInSAR) is an advanced version of InSAR in which two interferograms of the same ground surface are differenced from each other in order to separate out the phase information due to ground displacement. This phase information is used to measure the ground displacement at sub-millimeter accuracy, which has taken place between the two capture moments of the two interferograms.

Theory and applications of InSAR have been described extensively in existing literature, e.g., Gens and Vangenderen (1996), Bamler and Hartl (1998), Massonnet and Feigl (1998), Madsen and Zebker (1999), Rosen et al. (2000), Bürgmann et al. (2000), Rocca et al. (1997), to just mention a few. Here, we just intend to provide a basic overview of the working concept of InSAR.

Herrick (2012) describes the working concept as follows (cf. Figure 0-30): "As the satellite makes its first pass over a ground surface (*Initial ground surface*), it collects radar waves reflected off of the ground surface (solid wave, *pass 1*). During a subsequent orbit (often months to years later), when the satellite again passes over the same ground surface, another collection is made from very nearly the same orbital location (dashed wave, *pass 2*). If the ground surface deformed during the time between data collections (e.g., *subsided ground surface*), then the collected radar waves of the second pass will be out of phase compared to those collected during the first pass (example waves A-E, at right). The phase difference of the waves is then converted into the component of ground motion along the line-of-sight of the satellite (either towards or away from the satellite) and is represented by a colour as part of a full colour cycle. Since the technique is based on the phase difference of multiple waves, the accuracy is constrained by detectable fractions of the radar wave's wavelength".

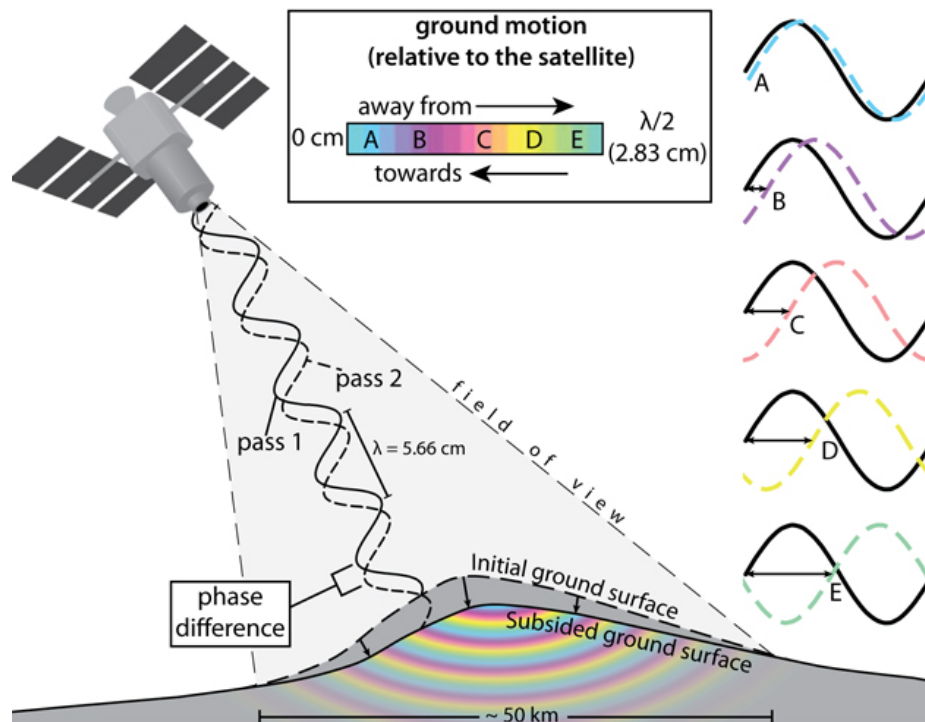


Figure 0-30: A cartoon representation of the basic principles of radar interferometry. Source: Herrick (2012), Image created by staff of the Global Volcanism Program. Downloaded from www.volcano.si.edu.

Due to the capability of measuring changes on the ground surface at very high accuracy InSAR is being efficiently used for monitoring and mapping of surface deformation. InSAR has also been successfully used for risk management in various applications, e.g.:

- **Landslides:** Changes in topography on landslide prone areas can be detected by identifying phase distortions in interferograms of long time spans with small baselines, which indicate possible mass displacements. A detailed investigation is needed for slow moving landslides using a series of interferograms ranging over time periods of a several months. Persistent Scatterer SAR Interferometry has been proven very fruitful for identifying very slow movement along slopes.
- **Earthquakes:** Ground surface changes due to seismic activity can be detected with the InSAR technique. Seismic movements can be investigated by deploying a network of corner reflectors to supplement the expensive ground survey from point-based GPS networking. Fault patterns are easy to identify from the fringe pattern in the interferogram(s).
- **Land subsidence:** Land subsidence takes place due to, e.g., mining activity, groundwater exploitation, petrol and gas abstraction, and CO₂ storage. Land subsidence phenomena from different activities contain a variety of temporal and spatial extents.

Some of the basic parameters used in SAR remote sensing are illustrated in Figure 0-31. Range direction is the horizontal direction in which the aircraft-/satellite-mounted antenna looks. It is generally perpendicular to the flight direction except in case of squint mode operation. *Ground range* is the distance away from the *nadir* point (perpendicular to the flight direction). *Slant range* is the

direct distance between the object and the sensor. The total distance from near range to far range imaged is known as swath width. Azimuth direction is the horizontal direction along the flight path. Pulse rectangle or footprint is the unit cell on the ground measured by the SAR. Angular relationship between antenna, incident ray and ground object are important factors in radar return. *Look angle* is the angle from the vertical to the beam measured in vertical plane. Look angle increases with increasing slant range, smaller at near range and larger at far range. Depression angle is complement to the look angle. Incident angle is the angle between incident ray and local vertical on the ground; it is a major factor influencing the reflectivity of the scatterers and varies inversely with the angle of incident.

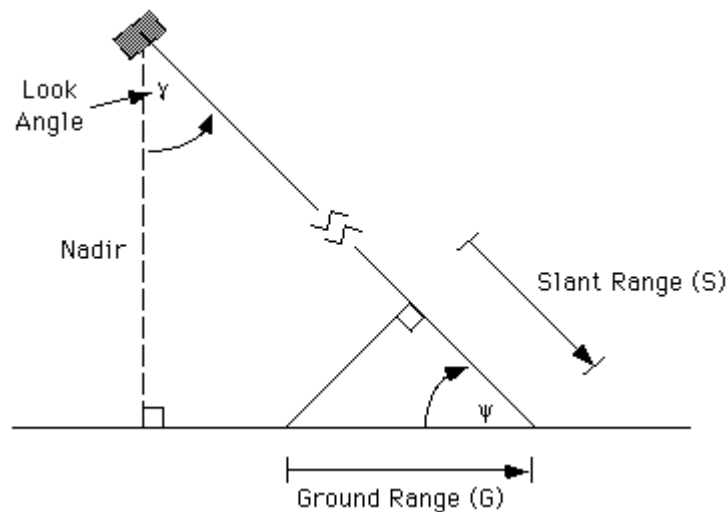


Figure 0-31: Working concept of SAR. Source: UAF Alaska Satellite Facility. Source: <http://www.asf.alaska.edu>.

A2. Spatial Resolution

Spatial resolution defines the ability of the SAR sensor to discriminate the closely spaced objects on the ground surface. It can be defined in terms of range and azimuth resolution illustrated in Figure 0-32, which are controlled by pulse-length and antenna-beam width respectively. The pulse length is determined by the length of the time that the antenna takes to emit its bursts of energy. Two objects will be resolved if the received pulse from the first object ends before that from the second object starts. The shorter the pulse length, the finer the resolution in range direction will be.

$$R_r = \frac{c\tau}{2 \cos\theta} \quad (1)$$

With

- c - Speed of light;
- τ - Pulse duration;
- θ - Depression angle.

Equation 1 shows that the range resolution also varies with the depression angle. It becomes finer from near range to far range. The azimuth resolution becomes coarser from near range to far range

because the beam width increases with the slant range. The azimuth resolution in Real Aperture Radar (RAR) can be expressed by beam width (β) and range (r).

$$R_a = \beta r \quad (2)$$

And the beam width can be expressed in terms of wavelength and physical length of the antenna.

$$\beta = \frac{\lambda}{D} \quad (3)$$

From Equation 2 and 3 it becomes clear that the azimuth resolution depends upon the wavelength of the system, the slant range and the antenna length. The range resolution depends upon the slant range and the reduction of the slant range can deteriorate the range resolution. Therefore, the azimuth resolution can be improved either by decreasing the wavelength or increasing the antenna length. Shorter wavelengths are more attenuated in the atmosphere, and therefore the azimuth resolution can only be improved by increasing the antenna length. However, on space-borne carrier systems there are limitations to improve the antenna length.

A3. Further principles of SAR Interferometry

Figure 0-33 shows the geometric configuration of InSAR. A_1 and A_2 are two SAR antennas working in repeating track mode viewing the same object on the ground, while their slant range distance is r and $r + \delta r$ respectively. The two antennas are separated by a baseline of length B and angle α with respect to horizontal. A_1 is located at height h with some reference surface. The topography H can be determined by phase measurement.

The phase delay measured at the antenna is proportional to the slant range given in Equation 4.

$$\varphi = \frac{2\pi}{\lambda} r \quad (4)$$

The difference of measured phase at antennas A_1 and A_2 is proportional to range difference (δr).

$$\Delta\varphi = \frac{4\pi}{\lambda} \delta r \quad (5)$$

The measured phase is modulo of 2π , which is required to be unwrapped for determining ground elevation information. Phase unwrapping is the process to find out absolute phase information from wrapped phase cycles. A number of algorithms have been proposed for phase unwrapping, among them most popular methods are Branch Cutting (Goldstein et al., 1988), Fringe Detection (Lin et al., 1994), Cellular-automation (Ghiglia et al., 1987) and Knowledge Injection (Adragna, 1995). From the imaging geometry shown in Figure 0-33 the topography height H can be derived by Equation 6:

$$H = h - r \cos\theta \quad (6)$$

where θ is the look angle of the radar.

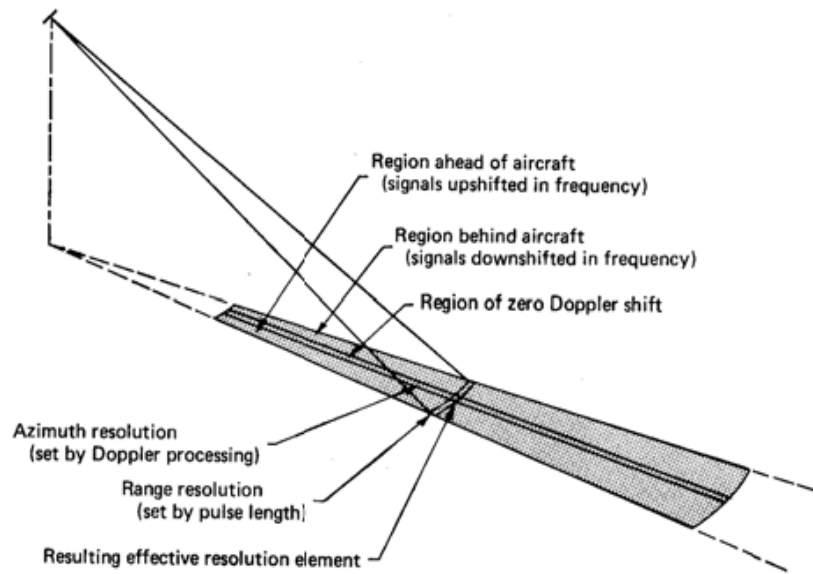


Figure 0-32: Determination of resolution in SAR system. Source: Franceschetti and Lanari (1999).

The measured phase of an interferogram is proportional to the parallel baseline. If we have a second interferogram of the same area over which no topographical changes occur, the phase difference in the second interferogram can be shown as:

$$\varphi_2 = \frac{4\pi}{\lambda} B'_{\text{par}} \quad (7)$$

The ratio of φ_2 and φ_1 is:

$$\frac{\varphi_2}{\varphi_1} = \frac{B'_{\text{par}}}{B_{\text{par}}} \quad (8)$$

The ratio of the phases in the two interferograms is equal to the ratio of the parallel baseline of the interferograms, i.e., independent to topography because radar wavelength is constant. A differential interferogram is produced by combining two interferograms and it is assumed that one interferogram possess only topography phase while the other one is characterized by both topography and displacement phase information. In this case the phase difference in the second interferogram will be:

$$\varphi_2 = \frac{4\pi}{\lambda} (r_1 + \Delta r - r) = \frac{4\pi}{\lambda} (B'_{\text{par}} + \Delta r) \quad (9)$$

The phase difference contains both topography and displacement phase values. If we subtract the topography phase values from the topographic phase, then only the displacement-generated phase will remain. Now we can find a solution that depends only on displacement generated phase change.

Since the slant range distance r is very much greater than the baseline it follows that the phase is much more sensitive for surface change detection than topography. With the interferometric technique, topography can be measured at some meters accuracy. Displacement can be measured at centimetre to millimetre accuracy. Therefore, the differential SAR interferometry can be used for measuring even small changes that occurred on the ground surface.

Differential interferograms can be obtained by using 3-pass or 4-pass interferometry and external DEM-eliminating methods. In 3-pass interferometry one image remains common in two differenced interferograms while in 4-pass interferometry four images are used to generate two interferograms. These two interferograms are subtracted to get final differential interferogram. In the DEM-eliminating method also called two-pass interferometry, one interferogram is generated using two SAR images and another interferogram is synthesized using an external DEM. This synthesized interferogram is subtracted from the original interferogram to obtain the differential interferogram.

A4. Image Coherence

Coherence is a measure of correlation between two images used for interferometric purpose that can be defined as the magnitude of interferogram pixels, divided by the product of the magnitudes of the original image's pixels. The mathematical coherence estimation is shown in Equation 10 (Rosen et al., 2000), where V_m and V_s are complex pixel values in master and slave image respectively and $E\{..}$ shows ensemble averaging.

$$\Delta = \frac{E[V_m V_s^*]}{\sqrt{E[|V_m|^2]E[|V_s|^2]}}, \quad 0 \leq \Delta \leq 1 \quad (10)$$

Theoretically, the value of coherence lies between 0 and 1. For fully coherent signals the value of Δ will be 1 and 0 for absolutely decorrelated signals. In general, it is rarely observed to have fully coherent or fully decorrelated signals. The correlation decreases with increasing volume scattering and temporal changes.

The phase information of SAR images to be combined should be coherent to make noise-free interferograms. Many factors add noise to interferograms and create image decorrelation:

- Temporal decorrelation,
- Geometric decorrelation,
- Baseline decorrelation,
- Data processing problems and
- Different atmospheric conditions during data acquisition.

The recorded phase information within a pixel shows the summation of the phases of all the backscattering elements that fall within a resolution cell dimension. If the relative changes in the position of backscattering elements within a pixel are greater than the radar wavelength than the pixel-by-pixel comparison of two images is not possible, which diminishes the suitability of InSAR for DEM generation. The elevation information obtained by interferograms depends on the phase measurement in slant range direction, which can be obliterated by temporal decorrelation. Decorrelation time can vary from a few hours in highly vegetated areas to several months in arid desert regions.

Foreshortening and layover are common phenomenon in SAR images of hilly terrain. Foreshortening takes place due to shortening of slant range at elevated points because elevated points displaced towards the satellite and compression of sloping terrain takes place, whereas layover occurs when the top of the slope is imaged earlier than the bottom of the slope. Geometrical decorrelation depends upon terrain slope angle and components of InSAR geometry. Layover is the extreme case of relief displacement, it occurs when the angle of slope facing towards the imaging satellite is

greater than look angle. Geometric distortion is inversely related with angle of incidence but shadows are pronounced.

Variation in the phase occurs with different viewing geometries, since the relative locations of the scattering cells depend on the viewing position. The different viewing geometries are denoted by the satellite baseline components and viewing angles. Satellite baseline position (both parallel and perpendicular) is illustrated in Figure 0-33, which shows the relative distance in the position of the satellite in the repeating orbit.

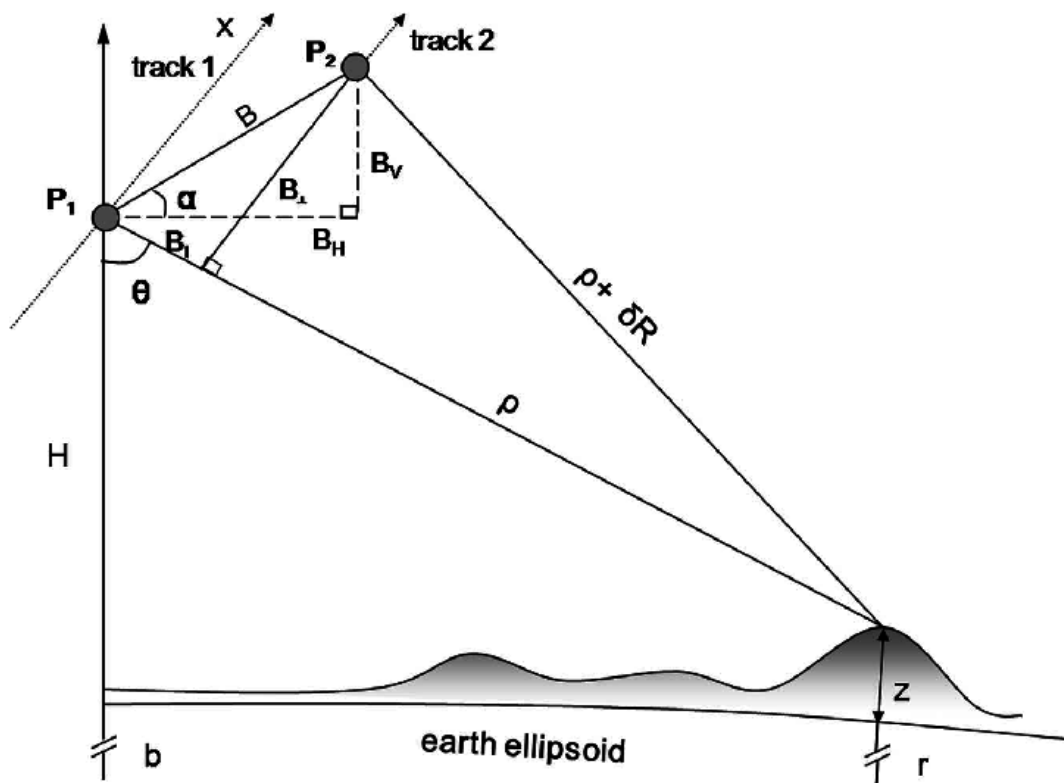


Figure 0-33: Viewing geometry of InSAR. Source: Baek et al (2008)

A less intuitive error source is baseline decorrelation that occurs because all targets within the resolution cell do not contribute to the same interferometric phase. Targets in the far range of the resolution cell will generally be viewed at an angle that is different from those in the near range. If the baseline is so large, that range resolution cells can take any value between $-\pi$ and $+\pi$, baseline decorrelation takes place and the resulting interferogram phase will be completely random. The baseline corresponding to this condition is referred to as the critical baseline (approximately 1100 m for ERS-1/2). Incorrect co-registration leads to decorrelation. Co-registration refers to the spectral and spatial alignment of two images so that they can overlay each other perfectly. The quality of the final interferogram is governed by the accuracy of co-registration; it must be accurate to within $1/8^{\text{th}}$ of a resolution cell to avoid phase error (EV-InSAR version 2.1, 2002).

Satellite radar signals are affected by atmospheric conditions. In repeat pass interferometry, the phase residues may be present due to atmospheric changes. Atmospheric effects can be removed using multiple interferograms. This is also the approach in using interferometric stacks and in

persistent scatterer-analysis (Ferretti et al., 2001). An atmospheric residue in the interferogram is independent from the baseline length. If many interferogram pairs of the same area at different baselines are available, then outliers can be identified by comparing the elevation variation along the range direction, which can be used to filter out the effect of atmospheric changes (Rocca et al., 1997).

A5. InSAR data processing

The SAR data processing steps (Figure 0-34) for DEM and displacement map generation can be summarized as described below.

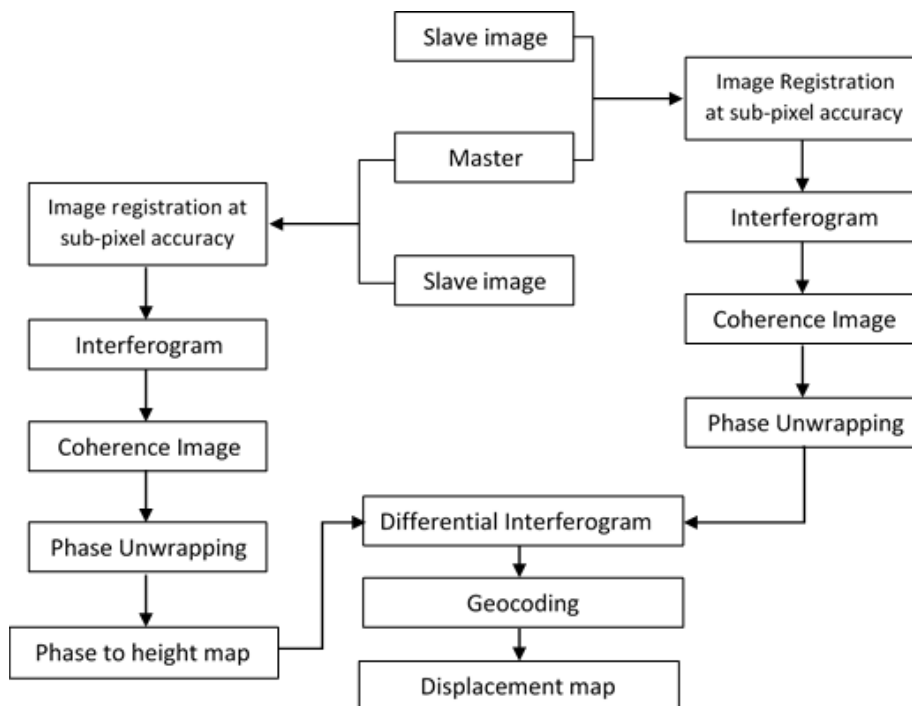


Figure 0-34: Flow diagram showing SAR data processing chain.

Data processing includes the following main steps:

- From two images, master and slave, the slave image is re-sampled both in range and azimuth directions to achieve accurate co-registration with the master image. Generally, the first obtained image is selected as the master image.
- An interferogram is generated from cross multiplication of master and slave images. Each pixel in interferogram shows the phase difference at that location, which is directly proportional to the range difference used to measure elevation information.
- The two images used for interferometric analysis are obtained from different viewing angles; due to this constant phase, value is added that is clearly visible in the interferogram as a series of fringes of constant phase running more or less parallel to azimuth direction. This extra phase value can be eliminated by subtracting constant phase value from interferogram that can be estimated from beat frequency. This extra phase removal is known as flat earth phase or residual phase removal.

- An interferogram contains the amplitude as well as phase information used for DEM generation. Measured phase difference between two images is modulus of 2π . Absolute phase value at each pixel is determined by phase unwrapping, see section 0.
- Geocoding is the process of assigning a particular geographic coordinate system to the maps and images so that the spatial information about the objects can be retrieved and a correlation between different maps and images can be established. It is necessary to transform range-Doppler coordinates of SAR image to the map coordinate system so that the information obtained from other map sources can be combined.

A6. InSAR stack processing

In order to overcome some of the above mentioned limitations of single pair interferometry, processing techniques have been developed to process large stacks/time series of images. There are two types of scattering mechanisms that can be considered for interferometric stacking: point scattering and distributed scatterers. For point scatterers, the backscatter is dominated by a single object, which is small in size compared to the resolution cell. For distributed scatterers, the backscatter is distributed evenly over the entire resolution cell. There two major techniques for processing InSAR stacks: Persistent scatterer InSAR (PS InSAR), which aims at identifying point scatterers and the Small Baseline Subset (SBAS) algorithm, which assumes distributed scattering. For stable results, rather long stacks of images are necessary for both techniques (~ 25 for PS and ~ 15 -20 for SBAS).

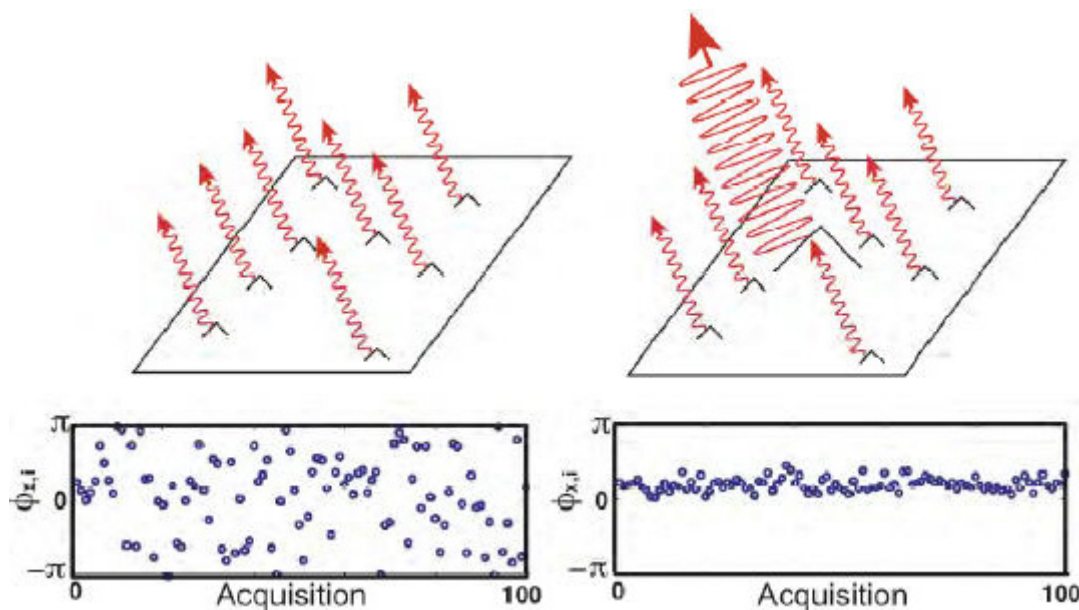


Figure 0-38 The main principle behind a PS. In a resolution cell, the signal will be a sum from many distributed point spreaders (left). For a PS, the reflected signal is dominated by one target in the resolution cell (right), making it independent of small differences in the look angle and temporal decorrelation, illustrated in the panel to the right (Hooper and Pedersen, 2007).

References Appendix A

- Adragna, F., 1995. "Production de MNT interferometriques sans deroulement de franges (resume)", Bulletin de la Societe Francaise de Photogrammetrie et Teledetection, pp. 138-145
- Baek, J., Kim, S.-W., Park, H.-J., Jung, H.-S., Kim, K.-D., and Kim, J.W. 2008. "Analysis of ground subsidence in coal mining area using SAR interferometry", Geosciences Journal, Vol. 12, No. 3, p. 277 – 284
- Bamler, R. and Hartl, P., 1998. "Synthetic aperture radar interferometry", Inverse Problems, vol. 14, pp. R1–54, 1998
- Bürgmann, R., Rosen, P. A., and Eric, J., 2000. "Fielding. Synthetic Aperture Radar Interferometry to Measure Earth's Surface Topography and Its Deformation", Annu. Rev. Earth Planet. Sci., vol. 28, pp 169–209
- Ferretti, A., Prati, C., and Rocca, F., 2001. "Permanent scatterers in SAR interferometry", IEEE Transactions on Geoscience and Remote Sensing, 39, pp 8-20
- Franceschetti, G. and Lanari, R., 1999. "Synthetic Aperture Radar Processing, CRC, Boca Raton, FL, pp. 25-28
- Gens, R. and Vangenderen, J. L., 1996. "SAR interferometry – Issues, techniques, applications," Intl. J. Remote Sensing, vol. 17, no. 10, pp. 1803–1835
- Ghiglia, D. C., Mastin, G. A., Romero, L. A., 1987. "Cellular-automata method for phase unwrapping", J. Opt. Soc. Am., vol. 4, pp. 267- 280
- Goldstein, R. M., Zebker, H. A., and Werner, C. L., 1988. "Satellite radar interferometry: Two-dimensional phase unwrapping", Radio Sci., vol. 23, no. 4, pp. 713-720
- Herrick, J., 2012. "Global Volcanism Program, Volcanic Activity Reports", Bulletin of the Global Volcanism Network, vol. 37, no. 5 (May 2012)
- Hooper, A., Pedersen, R., 2007. "Deformation due to Magma Movement and Ice Unloading at Katla Volcano, Iceland, Detected by Persistent Scatterer InSAR", Proceedings ENVISAT Symposium, Montreux
- Lin, Q, Vesecky, J.F., Zebker, H.A., 1994. "Phase unwrapping through fringe-line detection in synthetic aperture radar interferometry", Applied Optics, vol. 33, 201-208
- Madsen, S. N., and Zebker, H. A., 1999. "Synthetic aperture radar interferometry: Principles and applications," Manual of Remote Sensing. Boston, MA: Artech House, vol. 3, ch. 6
- Massonnet, D. and Feigl, K. L., 1998. "Radar interferometry and its application to changes in the earth's surface", Rev. Geophys., vol. 36, no. 4, pp. 441–500
- Rocca, F., Prati, C. and Ferretti, A., 1997. "An Overview of SAR Interferometry", Proc. 3rd ERS Symposium, Florence, <http://florence97.ers-symposium.org>
- Rosen, P. A., Hensley, S. and Joughin, I., Li, F., Madsen, S., Rodriguez, E., and Goldstein, R., 2000. "Synthetic Aperture Radar Interferometry", Proc. IEEE, pp. 333–379